Lectures 6-7

Valence Shell Photoelectron Spectroscopy

$.....np^6 \rightarrow ...np^5 + e$

$^1S_0 \rightarrow {}^2P_{3/2}$ or $^2P_{1/2}$

Two possible final states

Intensity is proportional to the Occupation numbers $(2J_1 +1)/(2J_2+1) = 4/2 = 2$

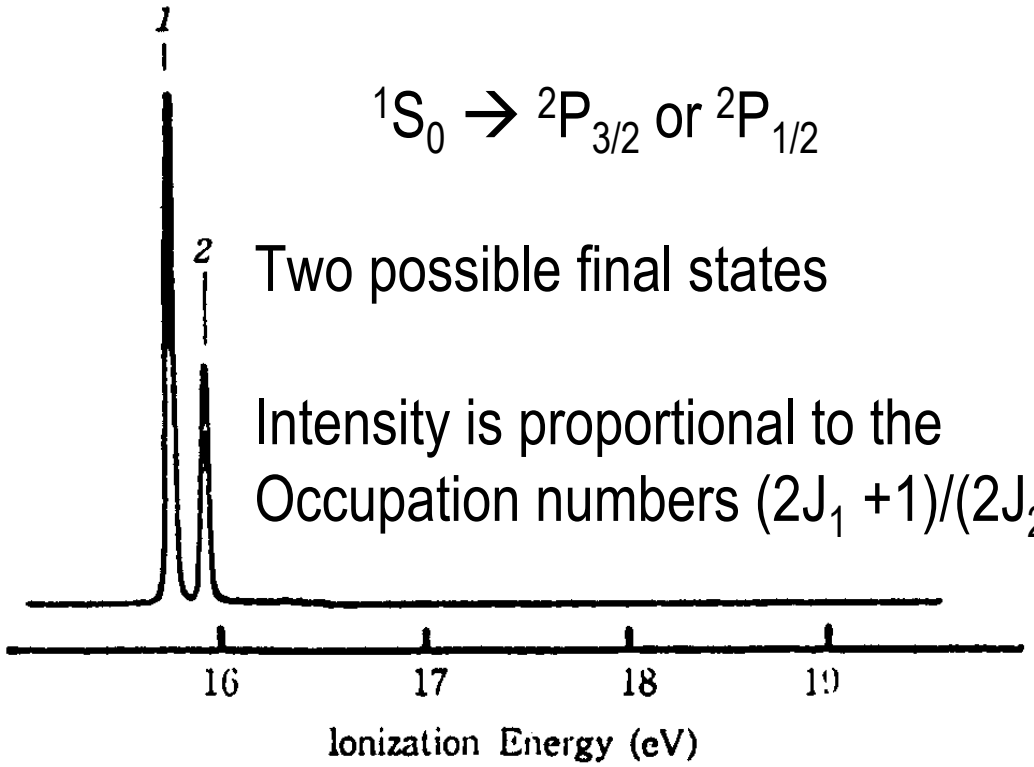

	Exptl.[a] I_v (eV)
1	15.759 ($^2P_{3/2}$)
2	15.937 ($^2P_{1/2}$)

a) The spectrum: this work. The I_v's: Turner *et al.* (215). See also other works: Carlson and Jonas (54); Kemeny *et al.* (126); and Branton *et al.* (37).

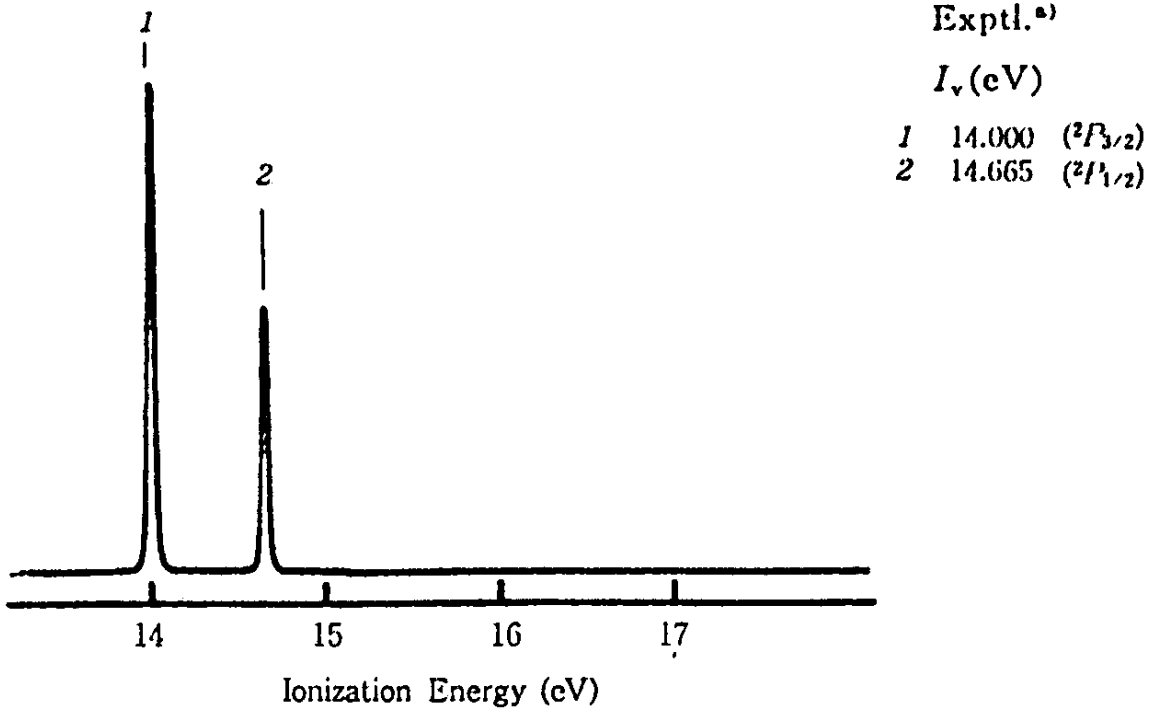

Exptl.[a)]

I_v(eV)

1 14.000 ($^2P_{3/2}$)
2 14.665 ($^2P_{1/2}$)

a) The spectrum: this work. The I_v's: Turner *et al.* (215). See also other works: Kemeny *et al.* (126); and Carlson and Jonas (54).

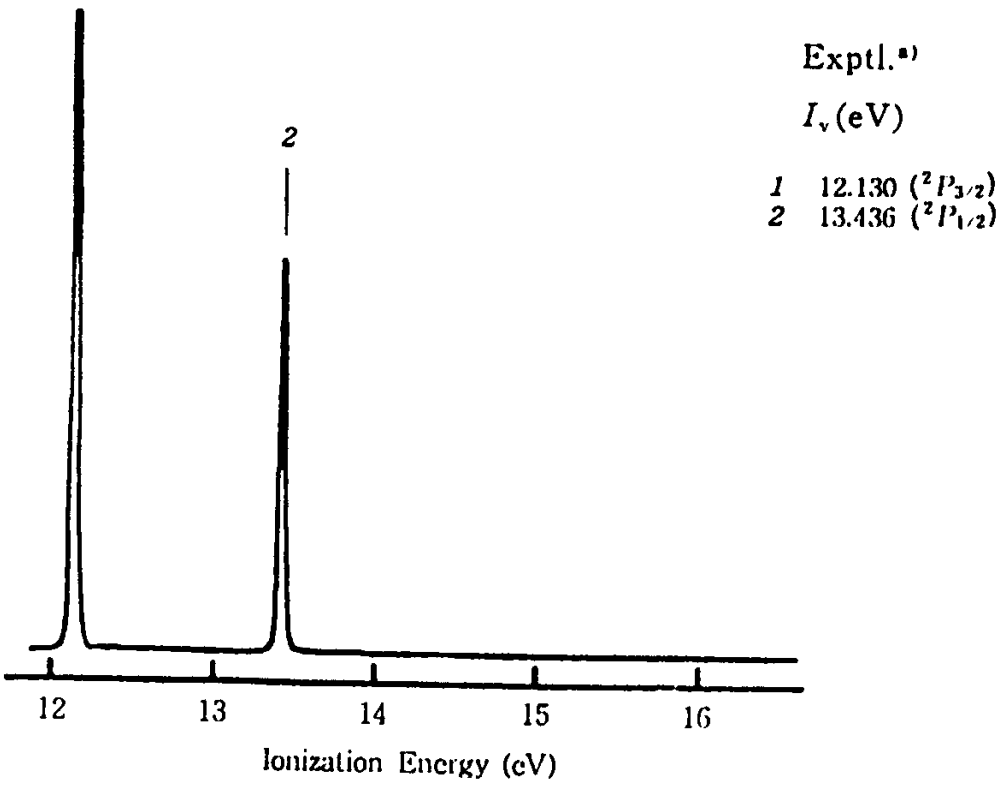

a) The spectrum: this work. The I_v's: Turner *et al.* (215). See also other works: Kemeny *et al.* (126) and Carlson and Jonas (54).

Spin-orbit coupling constant,

$\varsigma = [(Z\, e^2/8\pi\varepsilon_0\, m_e{}^2\, c^2)\, (Z/a_0)^3]/[n^3 l\, (l + ½)\, (l+1)\, hc]$

$= \alpha^2\, R_\infty\, Z^4/[n^3\, l(l+1/2)\, (l + 1)]$;
proportional to Z^4

α- fine structure constant

$e^2/[4\pi\varepsilon_0 \hbar C] = 1/137.03604$

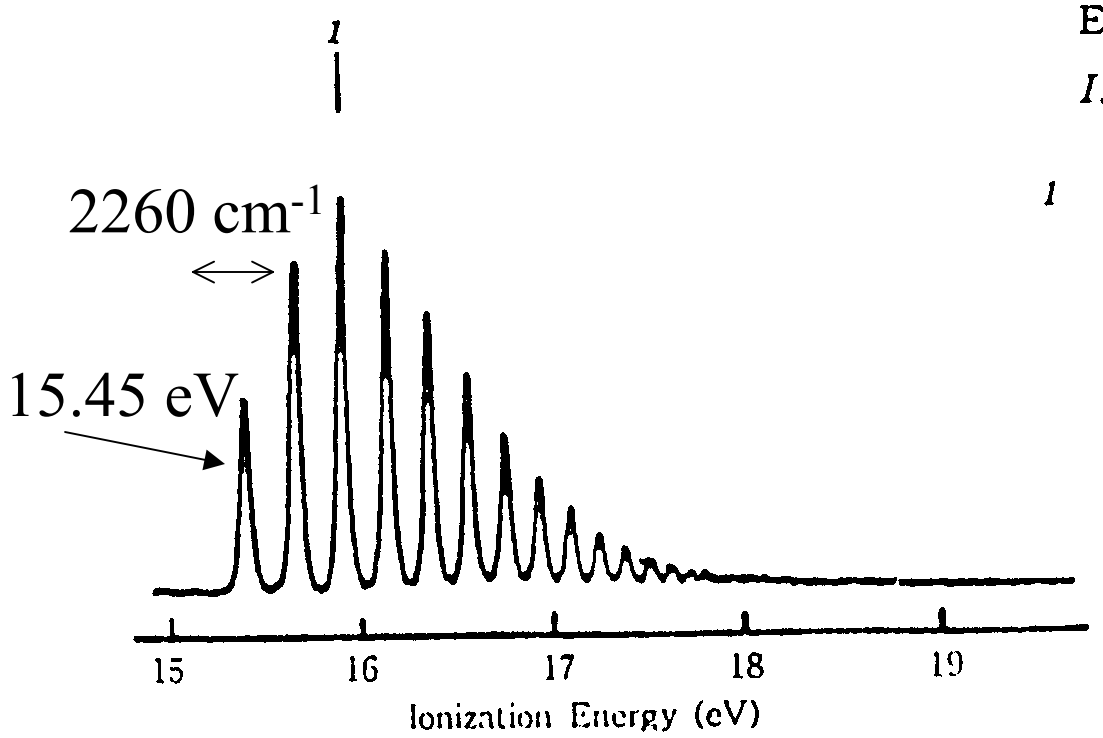

Exptl.[a)]

I_v (eV)

1 15.98

a) The spectrum : this work. The *Iv*'s : Turner and May (215a). See also other works : Turner (214) ; Turner *et al.* (215) ; Åsbrink (3) ; Cornford *et al.* (67) ; Niehaus and Ruf (167) ; Shaw and Berry (204) ; Carlson and Jonas (54) ; Berkowitz and Spohr (23) ; and Lee and Rabalais (149).

Vibrational Structure

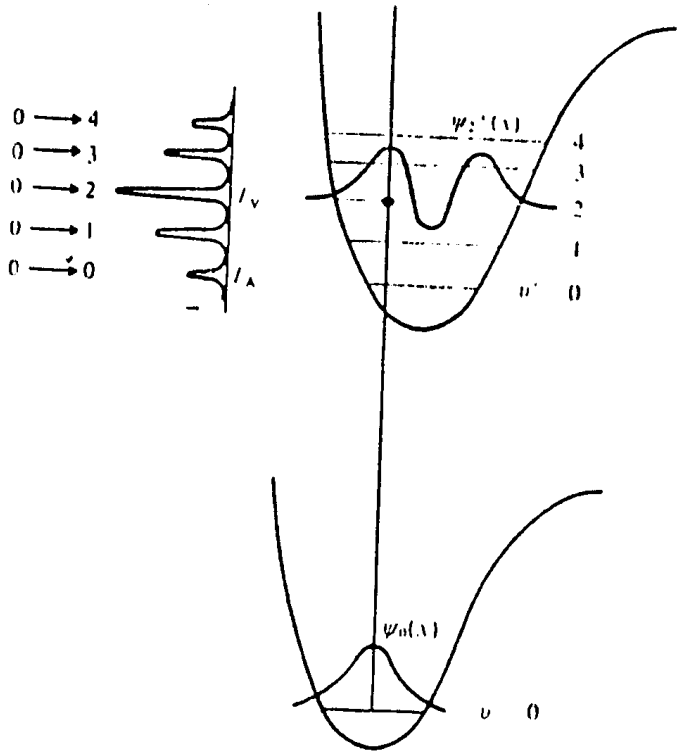

Figure 20.12 Potential energy curves for a molecule and one of its ionized states, illustrating the 'vertical' nature of the photoionization process and the production of the molecule-ion in different vibrational states.

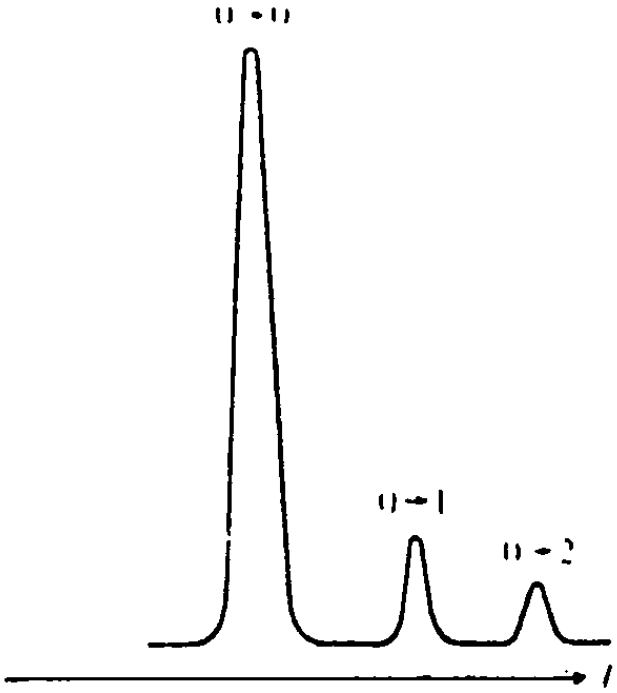

Figure 20.13 The form of the vibrational fine structure of a PE band when photoionization occasions very little change of molecular dimensions

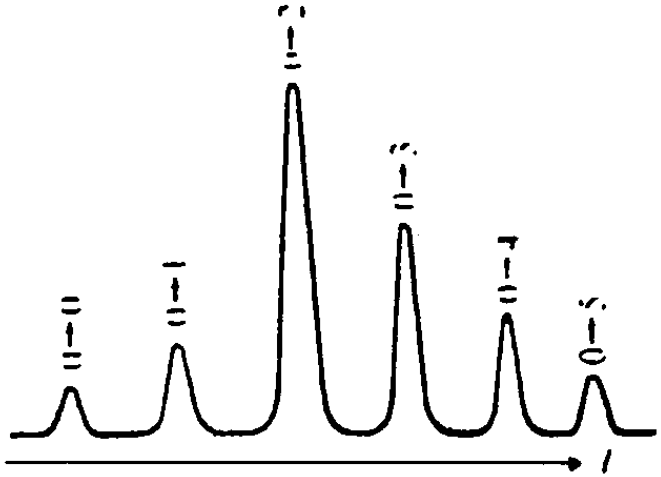

Figure 20.14 Typical vibrational line structure for a PE band when there is a significant change in molecular dimensions upon photoionization.

(7) N_2 Nitrogen

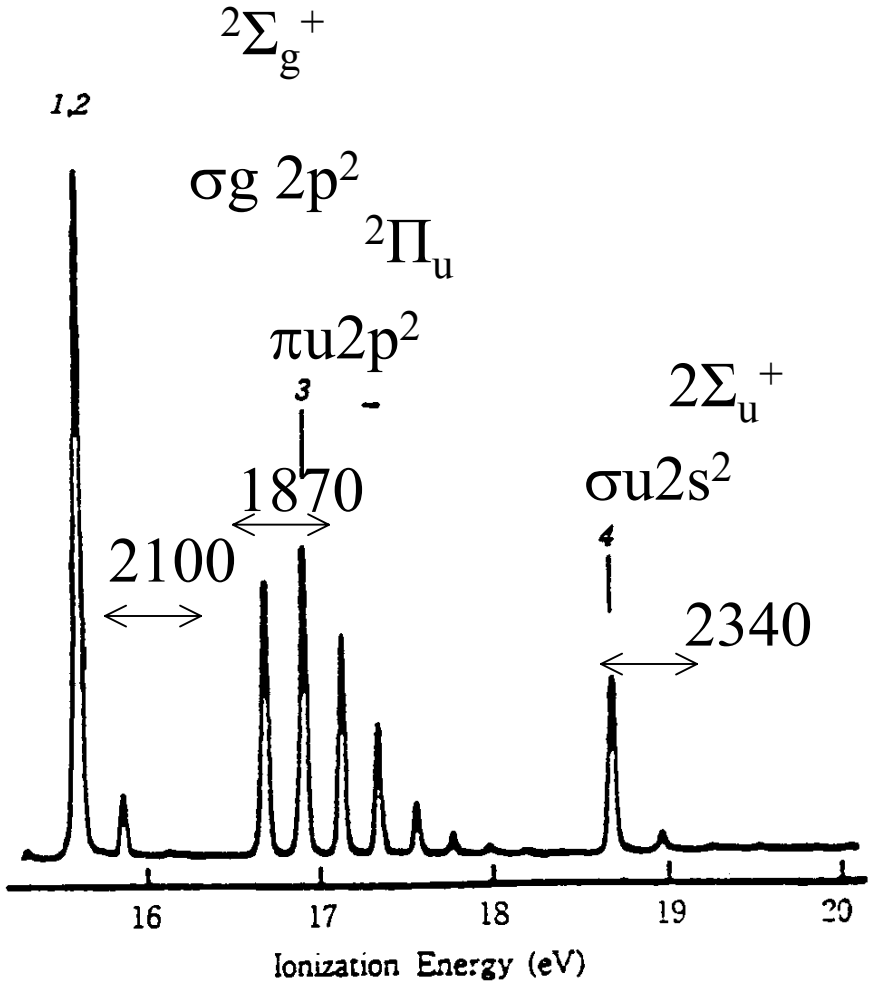

Adiabatic 15.57 16.69 18.75 eV

Franck – Condon Factor

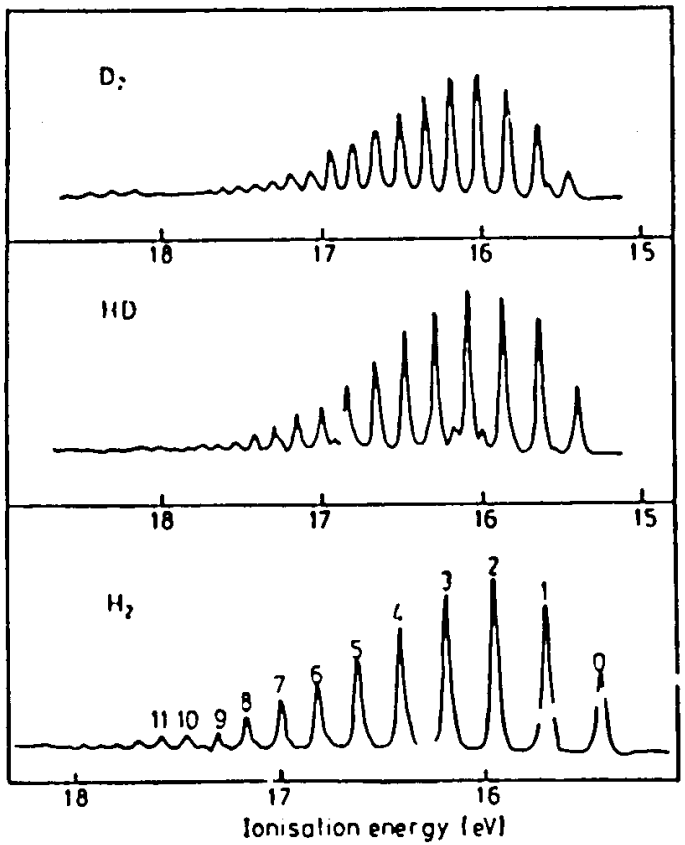

Figure 26.1. Photoelectron spectra of D_2, HD and H_2 obtained using He resonance radiation. The numbers in the H_2 spectrum denote the vibrational quantum number of the ionised state (Berkowitz and Spohr 1973).

Dipole approximation, probability $\alpha \langle\phi|er|\varphi^{+}|\rangle^2$

$\phi = \Psi\Theta$ Born – oppenheimer approximation

$\langle \phi|er| \phi^{+}\rangle = \langle\Psi|er| \Psi^{*}\rangle \langle\Theta|\Theta\rangle$

er is electronic operator, acts only on the electronic part of the wave function.

Franck – Condon factor $\langle\Theta|\Theta\rangle^2$

FC factors predict intensities accurately. Deficiencies due to neglect of rotations, neglect of polarisation of ion by photoelectron, deviation of neutral molecule from equilibrium geometry by zero point motion and failure of Born – Oppenheimer approximation

Table 26.1. Ionisation energies, experimental intensities and calculated Franck–Condon factors for the ionisation of H_2, HD and D_2 (Berkowitz and Spohr 1973, Gardner and Samson 1976)

Molecule	n(ion)	I(eV)	Experimental intensity (Berkowitz and Spohr 1973)	Experimental intensity (Gardner and Samson 1976)	Franck–Condon factor (Gardner and Samson 1976)
H_2	0	15·4254	0·463	0·448	0·521
	1	15·6971	0·863	0·922	0·918
	2	15·9530	1·000	1·000	1·000
	3	16·1936	0·884	0·969	0·879
	4	16·4194	0·700	0·713	0·689
	5	16·6308	0·579	0·572	0·508
	6	16·8281	0·472	0·423	0·361
	7	17·0113	0·313	0·308	0·253
	8	17·1808	0·241	0·208	0·176
	9	17·3365	0·137	0·132	0·122
	10	17·4783		0·089	0·085
	11	17·6061		0·058	0·060
	12			0·039	0·042
	13			0·024	0·030
	14			0·015	0·021
	15			0·005	0·014
HD	0	15·444	0·300		0·402
	1	15·682	0·676		0·818
	2	15·907	1·000		1·000
	3	16·120	0·975		0·965
	4	16·329	0·963		0·816
	5	16·515	0·810		0·638
	6	16·710	0·634		0·475
	7	16·880	0·407		0·344
	8	17·040	0·264		0·245
	9	17·185	0·218		0·173
	10	17·330	0·160		0·123
D_2	0	15·466	0·230		0·260
	1	15·664	0·538		0·648
	2	15·854	0·812		0·940
	3	16·032	0·950		1·048
	4	16·206	1·000		1·000
	5	16·371	0·928		0·864
	6	16·528	0·756		0·699
	7	16·680	0·624		0·541
	8	16·824	0·487		0·407
	9	16·962	0·342		0·300
	10	17·087	0·270		0·219

Vibrational Interval

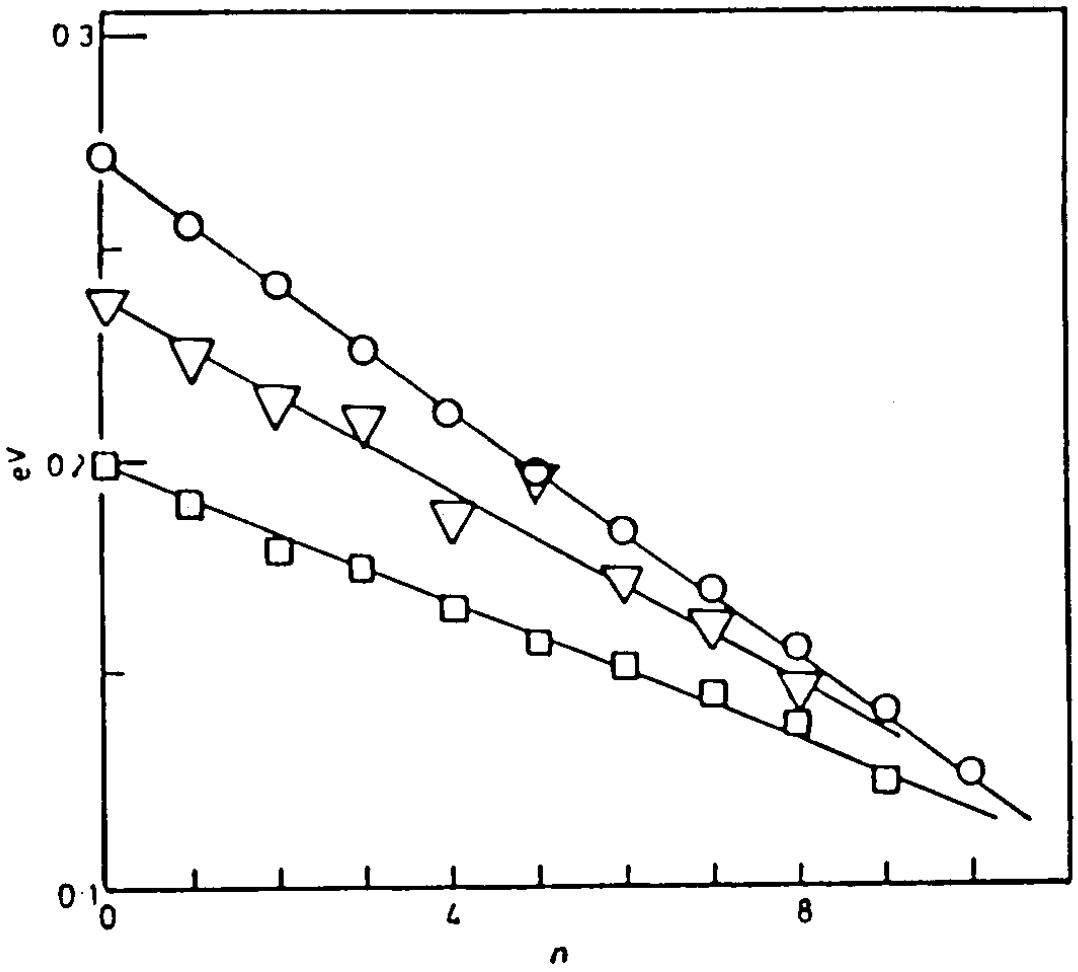

Figure 27.1. Plots of the vibrational interval against the vibrational quantum number, n, for the $^2\Sigma_g^+$ bands of H_2, HD and D_2. O H_2; V HD; □ D_2.

For H_2^+, D = 2.648 eV

$D = 12\ \omega_0 n_D$

For H_2^+ $n_D = 19$ and $\omega_0 = 0.2712$

$D = 1/2 \times 19 \times 0.2712$

$= 2.58$ eV

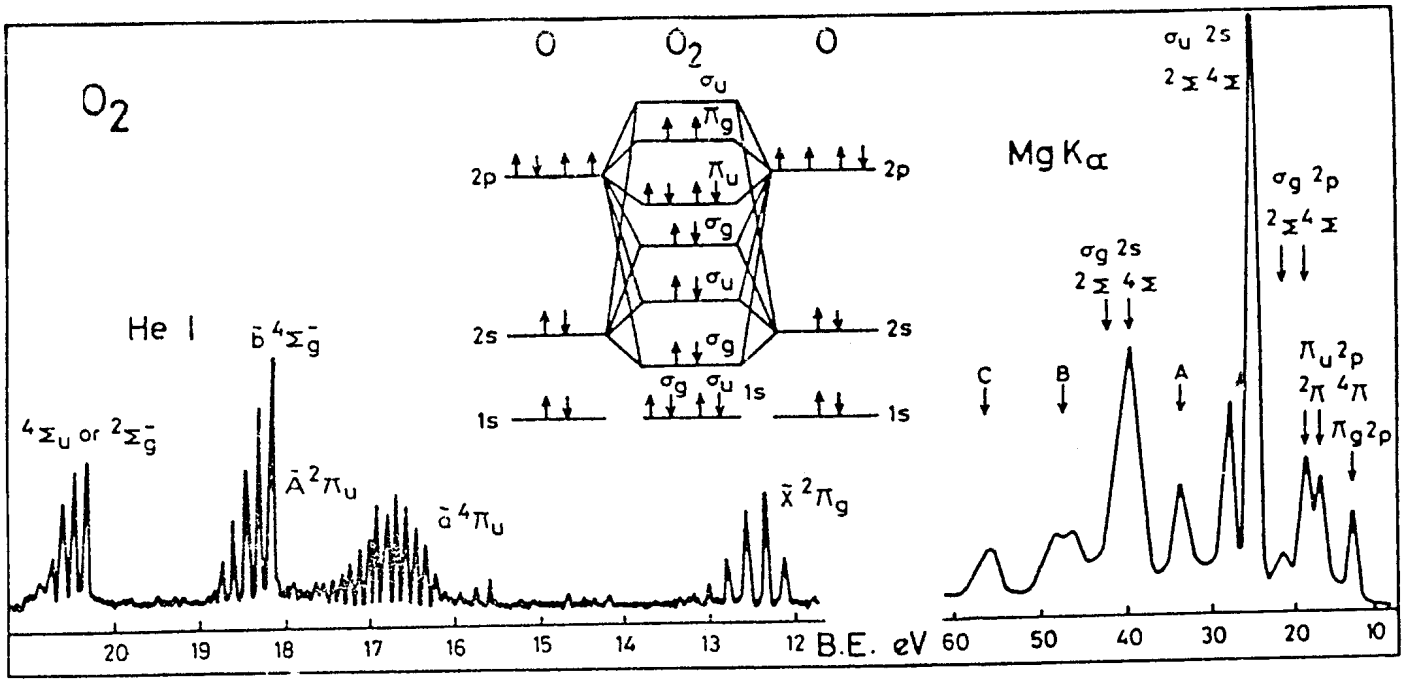

Fig. 4.2. Valence electron spectra of oxygen using HeI and Mg K_α sources [4, 5].

Spin multiplicities

$\pi_g \alpha p \rightarrow {}^2\pi$

$\pi_n \alpha p \rightarrow {}^2\pi, {}^4\pi$

Energy loss shake up

$\Delta\nu_v \approx 400\ cm^{-1}$
$hf \quad 1780\ cm^{-1}$

Figure 20.18 The first band in the PE spectrum of O_2 excited by Ne I ($h\nu$ = 16.85 eV) radiation. (The spectrum has been stripped of equivalent structure due to ionization by the less intense Ne I line having $h\nu$ = 16.67 eV.)

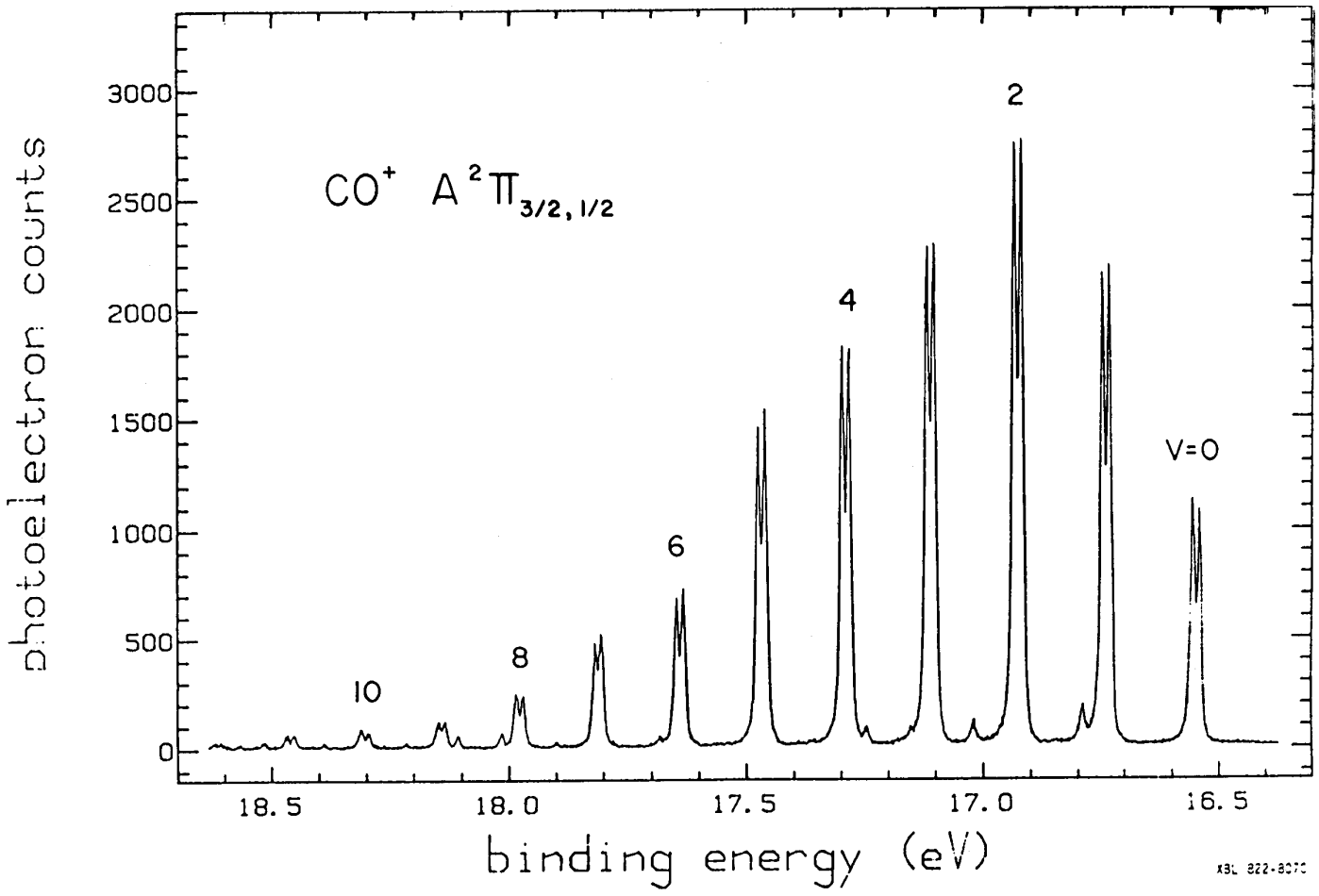
photoelectron counts
3000
2500
2000
1500
1000
500
0
CO^+ $A^2\Pi_{3/2,1/2}$
10
8
6
4
2
V=0
18.5
18.0
17.5
17.0
16.5
binding energy (eV)
XBL 822-8070

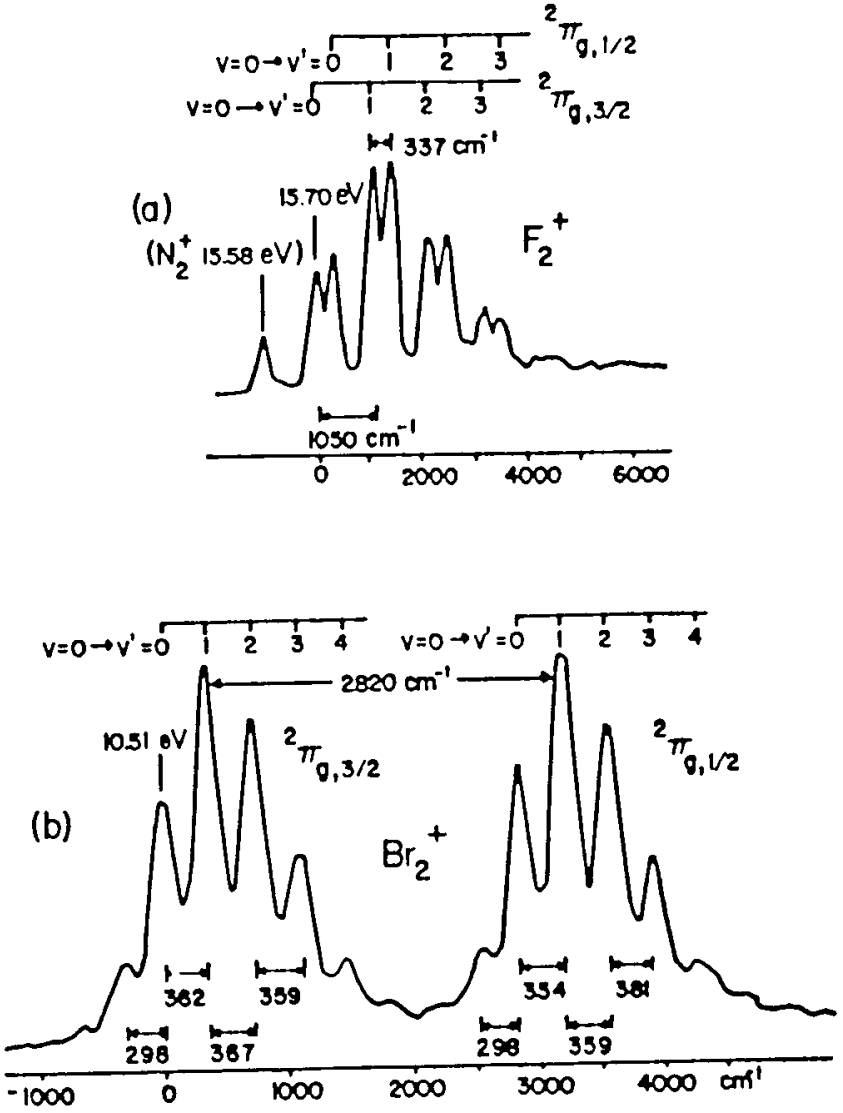

Fig. 5-18. He I photoelectron spectra of (a) F_2 and (b) Br_2, showing fine structure of the lowest ionic states. From A.B. Conford, D.C. Frost, C.A. McDowell, J.L. Ragle, and I.A. Stenhouse, *J. Chem. Phys.*, *54*, 2651 (1971).

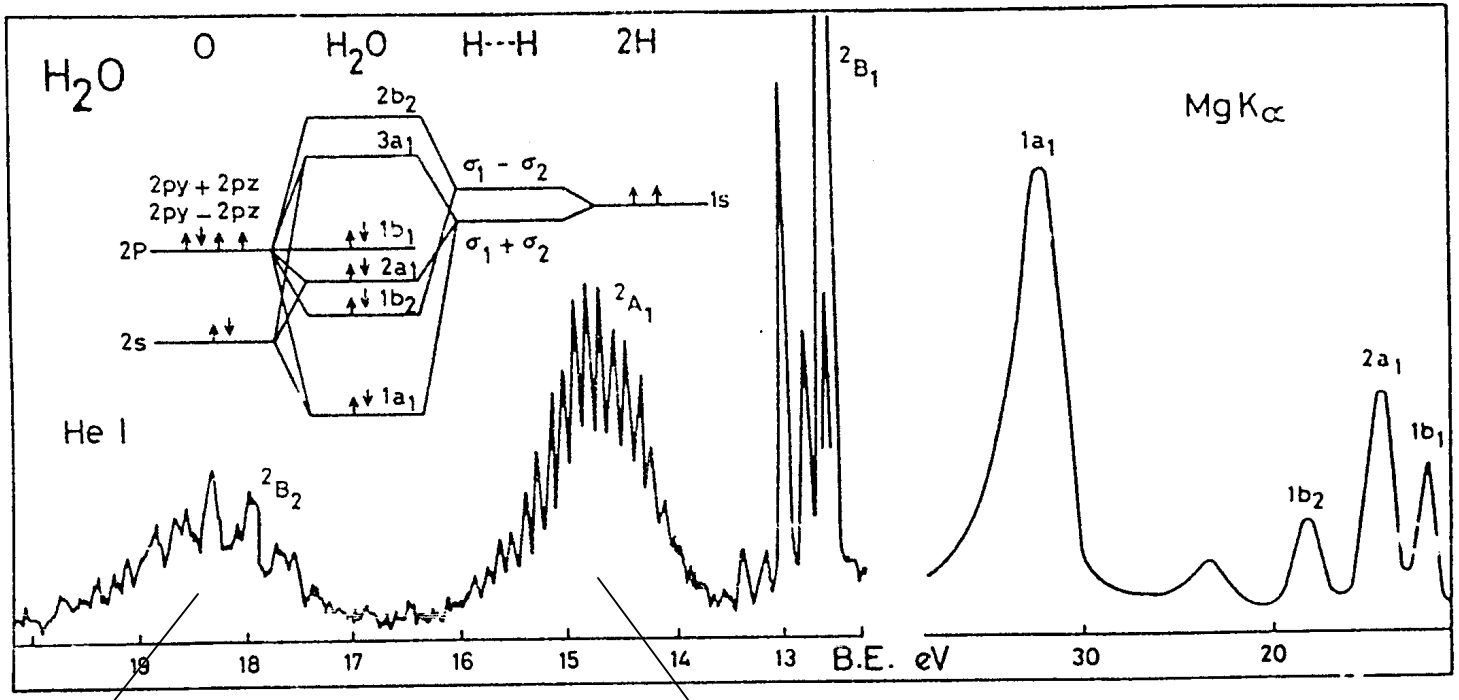

Fig. 4 3. Valence electron spectra of water using HeI and Mg K_α sources [4, 5].

Life time

H – H anti bonding

υ_2 increases (bonding)

υ_1 decreases (stretching)

Bonding υ_2

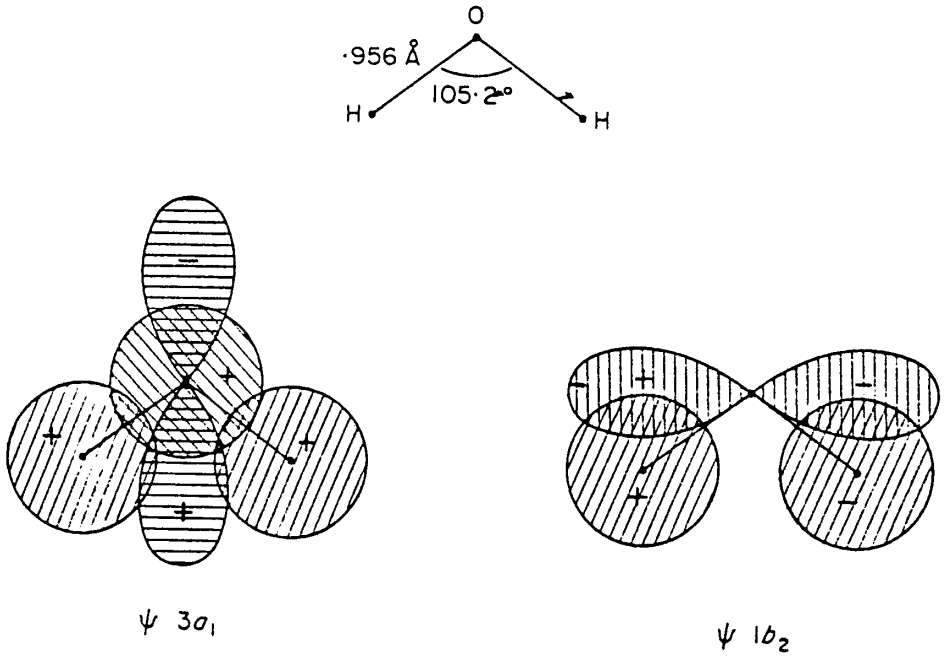

Figure 4.33 The occupied orbitals of the water molecules illustrated in terms of their constituent atomic orbitals

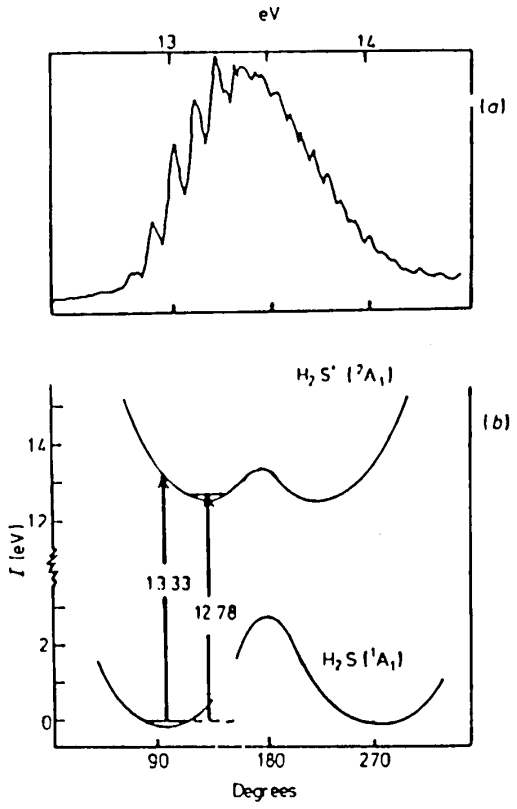

Figure 32.2. (*a*) The photoelectron spectrum of H_2S in the region of ionisation of the $3a_1$ electron'c orbital (cf figure 17.2). The inversion barrier is surmounted at 13·3 eV, where a halving of the vibrational interval is seen (Potts and Price 1972). (*b*) Schematic potential energy plot of the ground state of H_2S and he $3a_1^{-1}$ state of H_2S^+. The adiabatic and vertical ionisation energies are shown.

Vibrational Inversion

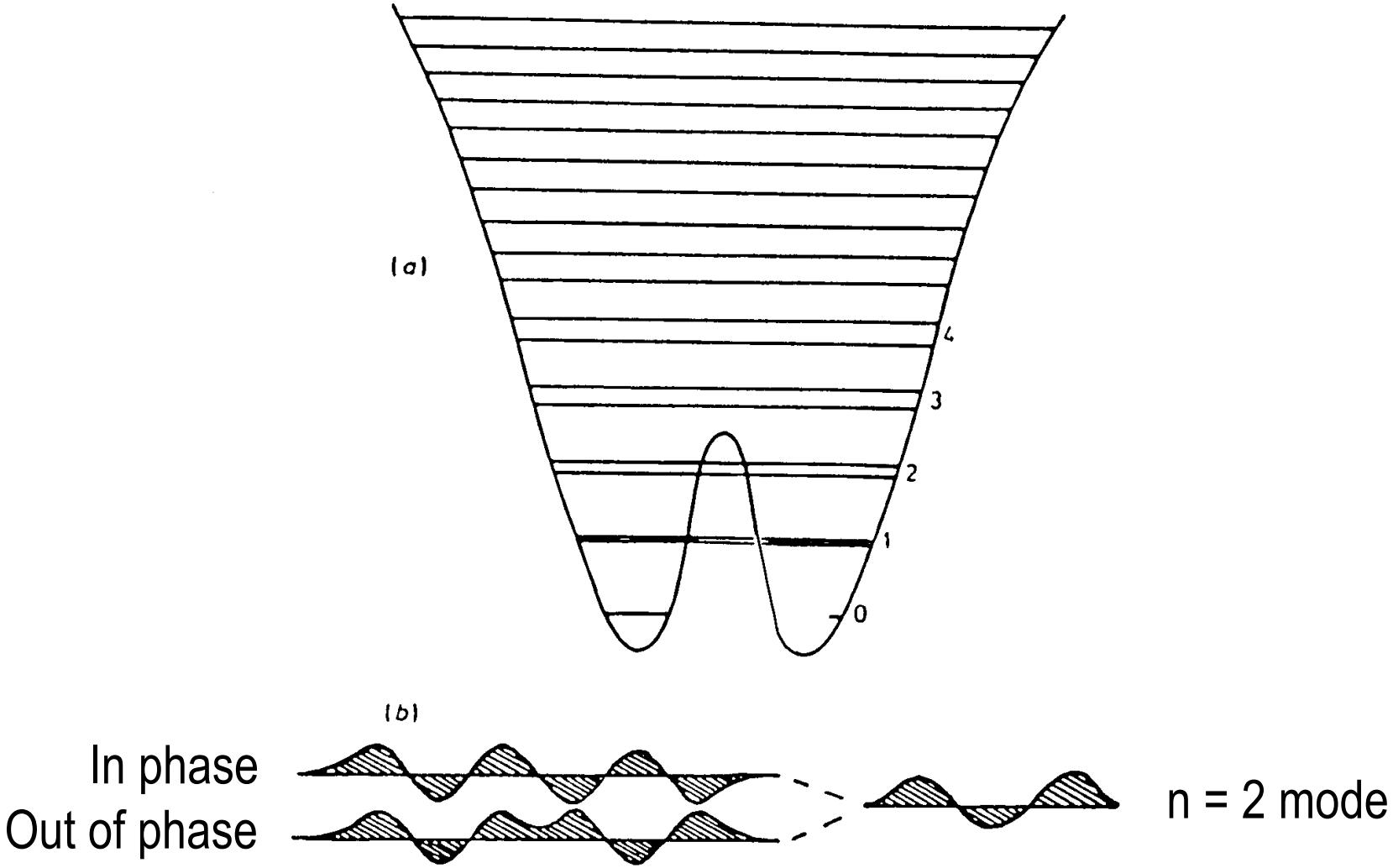

Figure 32.1. (*a*) Potential energy curve in the presence of an inversion mode of vibration. (*b*) On the right-hand side is drawn the $n = 2$ vibrational mode, and on the left-hand side a pair of the same modes have interacted in-phase and out-of-phase. Interaction takes place near and above the central barrier to inversion.

No interaction when n = 0. At high amplitudes the wavefunctions mix either in phase or out of phase. A pair produces two independent functions which are non degenerate.

H_2S, H_2O $3a_1$ linear, H_2Se, H_2T_e
887 cm^{-1} Vs 1595 cm^{-1}

NH_3, PH_3, AsH_3, Sb H_3

950 (NH_3) 992 (PH_3)489; 906 (A_3H_3)452 ; 781 (SbH_3) 387

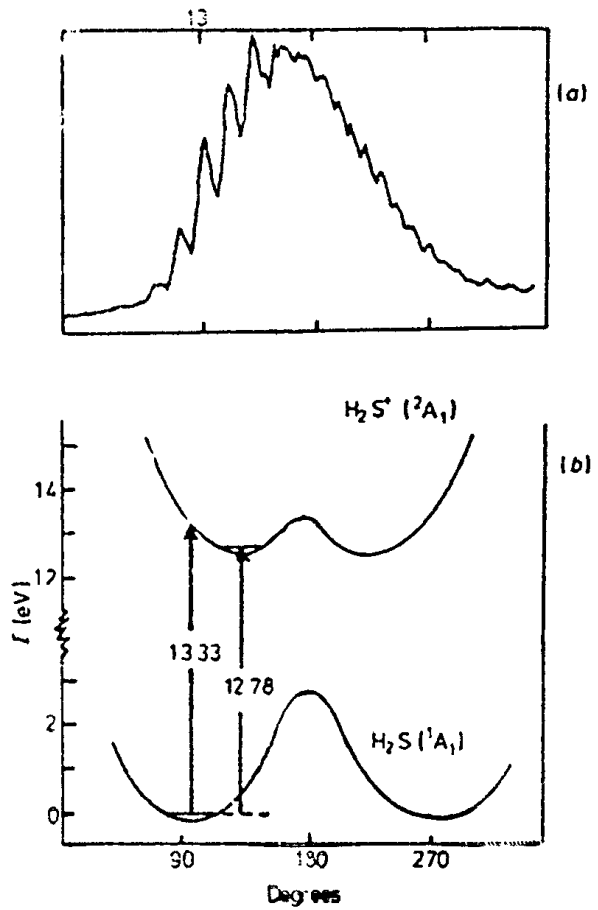

Figure 32.2. (*a*) The photoelectron spectrum of H_2S in the region of ionisation of the $3a_1$ electronic orbital (cf figure 17.2). The inversion barrier is surmounted at 13·3 eV, where a halving of the vibrational interval is seen (Potts and Price 1972). (*b*) Schematic potential energy plot of the ground state of H_2S and the $3a_1^{-1}$ state of H_2S^+. The adiabatic and vertical ionisation energies are shown.

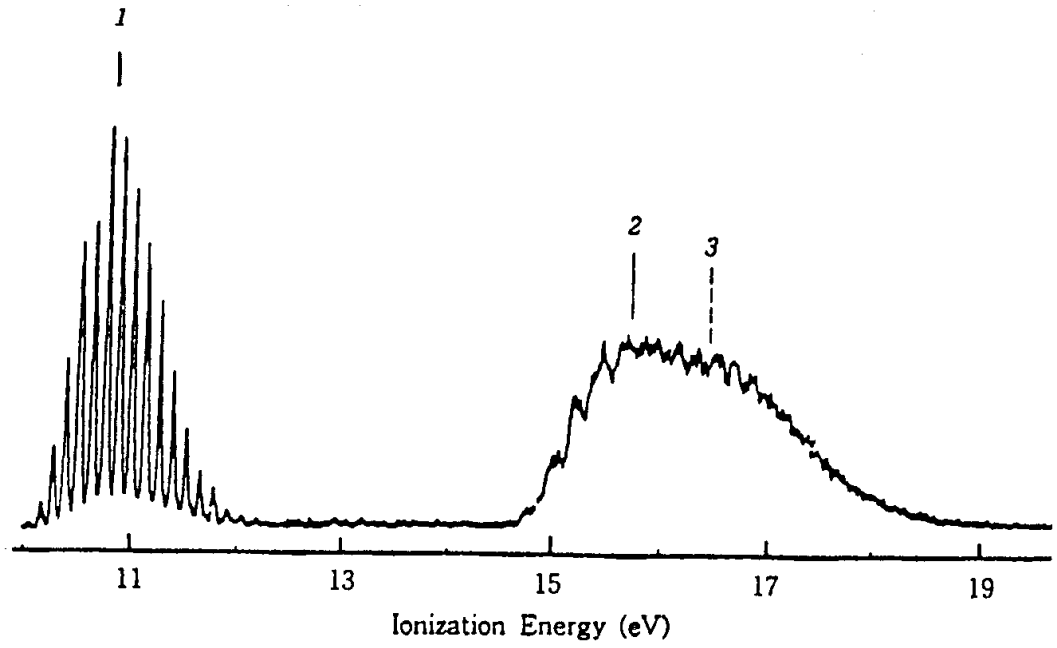
1
2
3
11
13
15
17
19
Ionization Energy (eV)

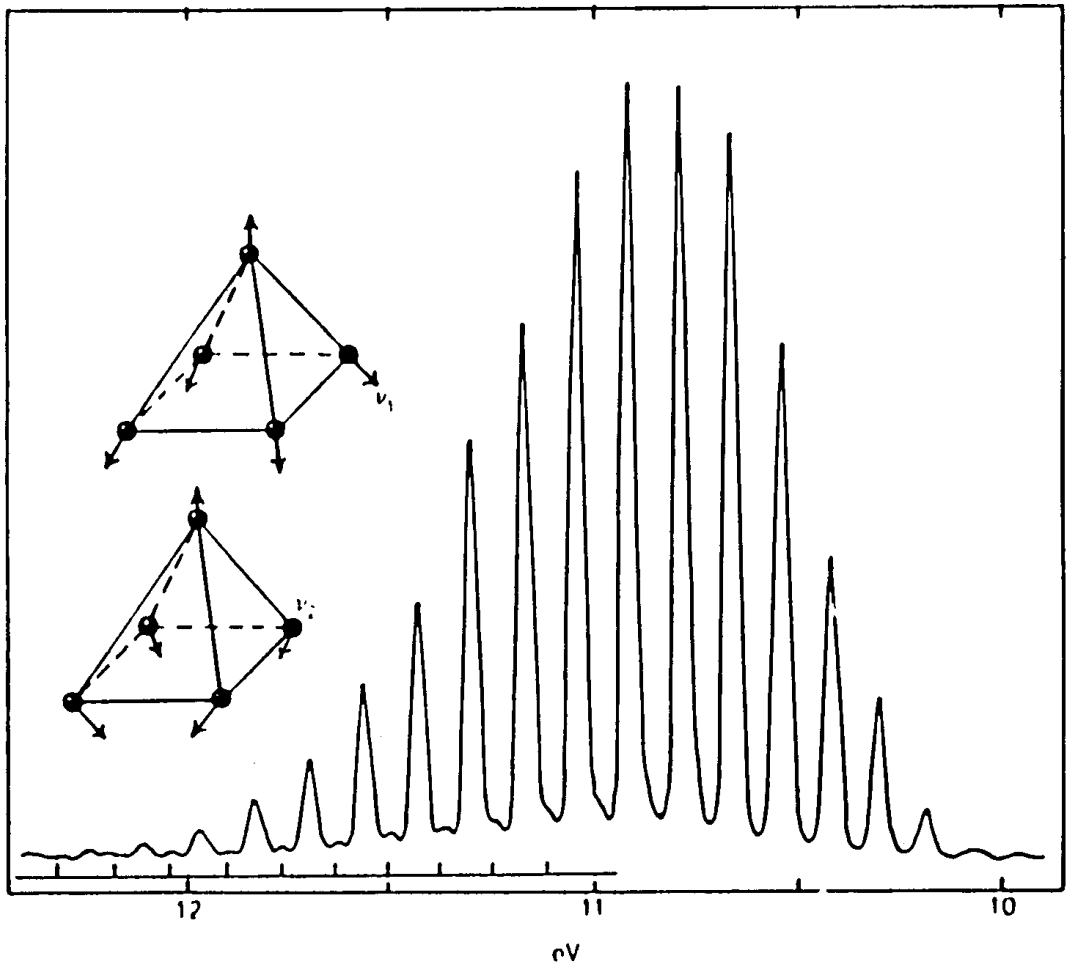

Figure 32.3. The photoelectron spectrum of ammonia in the region of ionisation of the $3a_1$ band (cf figure 17.2) showing two progressions of the inversion mode, ν_2. The weaker of the two progressions is picked out by the vertical bars at the lower left of the figure; this probably arises from one quantum of ν_1 plus the ν_2 quanta (Rabalais *et al* 1972).

Jahn – Teller effect

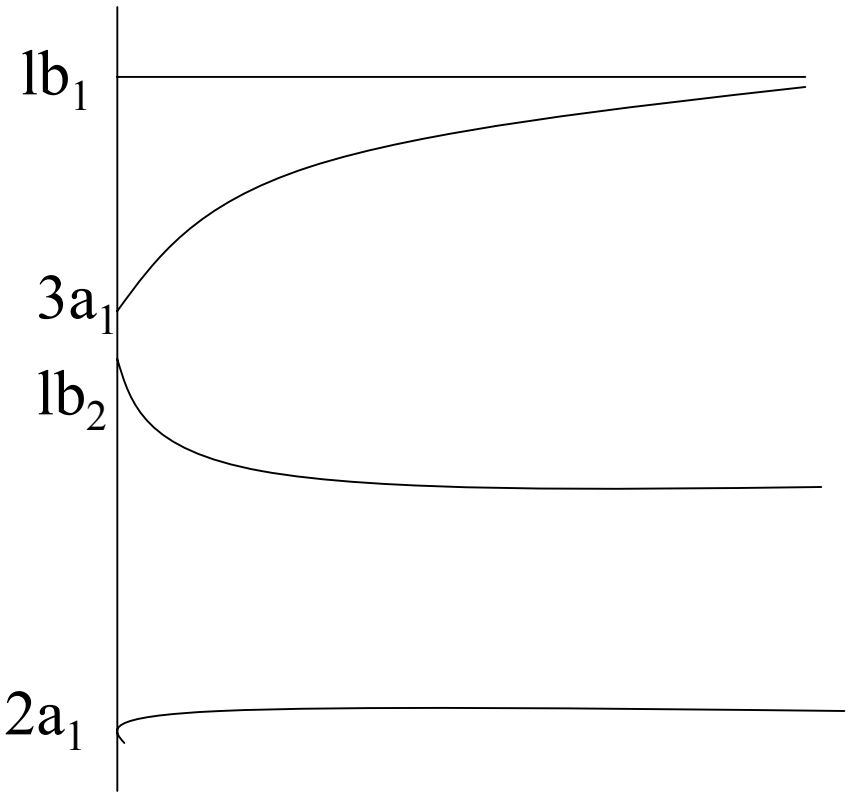

Walsh diagram of water

Static and dynamic Jahn-Teller effects

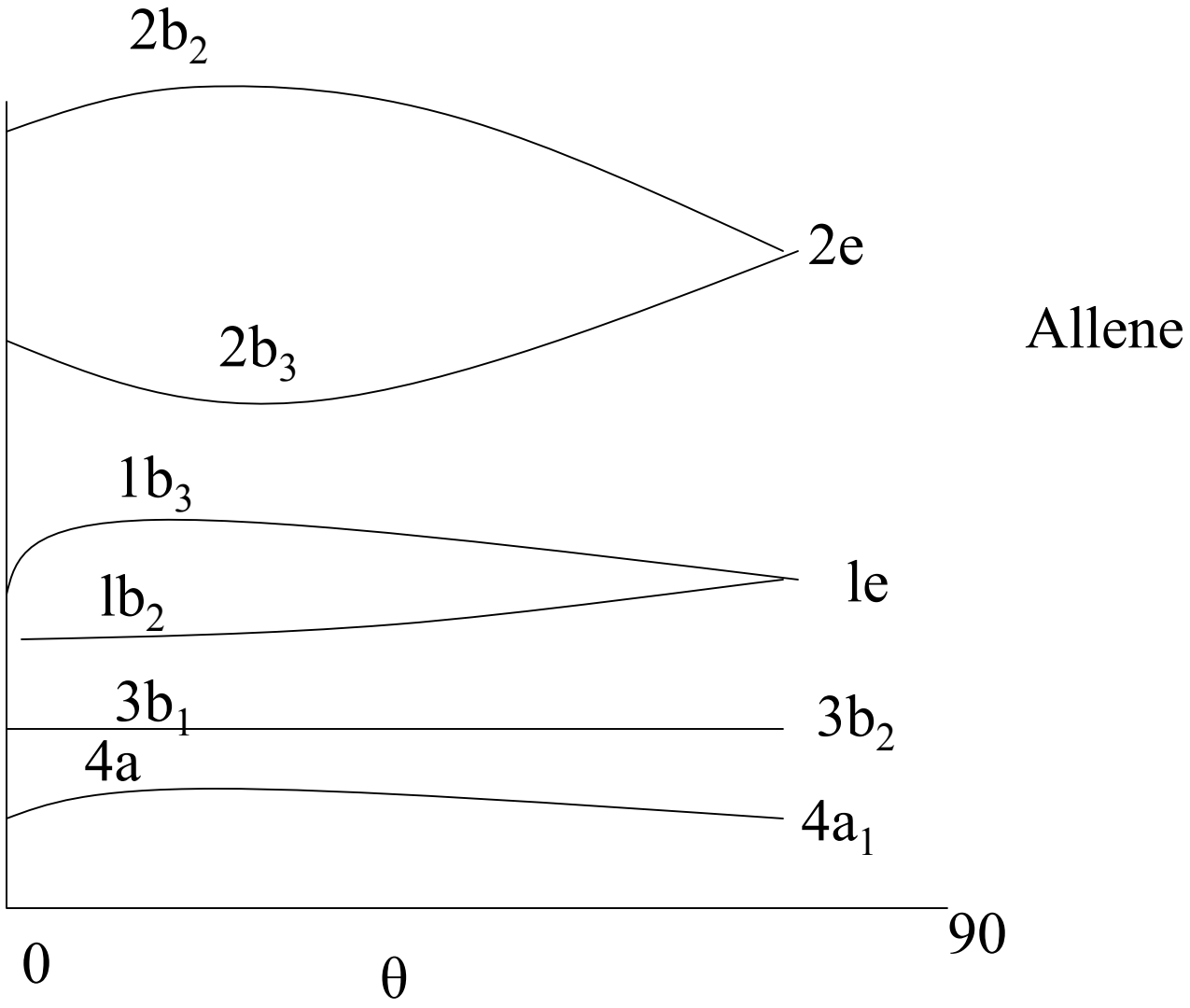
2b2
2e
2b3
Allene
1b3
1e
1b2
3b1
3b2
4a
4a1
90
0
θ

b_2 C – C – C asymmetric stretch $\rightarrow C_{2v}$
b_1 torsional mode $\rightarrow D_2$ (except when $\theta = 0$ which makes it to D_2h)

Jahn – Teller splitting of 2e ~ 0.6 eV.
Which means θ to decrease by 12^o.

Calculations indicate that $\theta = 38^0$ in the $2e^{-1}$ state

1e splits only to a lesser extent

Jahn – Teller active vibrations

$\langle \Psi_i | H_0 | \Psi_j \rangle = E_0$ if $i = j$

$H = H_0 + \nu' Q + \nu'' Q^2 + \ldots$ Q = displacement vector

Q leads to new eigenfunctions.

$\xi_i = \Sigma C_i \Psi_i$

Neglecting higher order terms, this gives secular equations,

$$\begin{vmatrix} H_0 - E & \nu' Q \\ \nu' Q & H_0 - E \end{vmatrix} = 0$$

$E = Eo \pm \langle \Psi_1 | \nu' Q | \Psi_2 \rangle$

If the second term is finite, the energy levels split. This will happen if the direct product of Ψ_1 and Ψ_2 contains an reducible representation as Q.

For the D_{2d} point group, (e x e) direct product gives A_1, A_2, B_1 and B_2. Thus A_2, B_2 and B_1 vibrations can be John-Teller active.

A_2 is not a pure vibration, it has rotational symmetry.

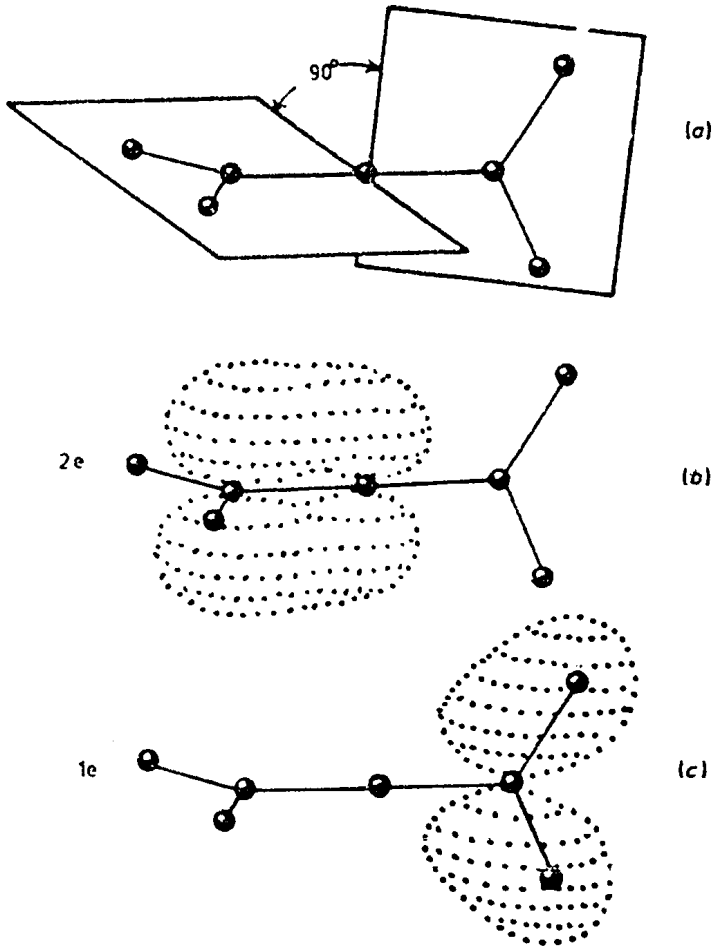

Figure 33.2. (*a*) The equilibrium geometry of allene. The C–C–C assembly is linear and the dihedral angle, θ, between the planes defined by the CH_2 groups is 90°. The point group is D_{2d}, and the x axis lies perpendicular to the C–C–C axis and bisects the dihedral angle. (*b*) and (*c*) Lobes of the molecular orbitals of e symmetry.

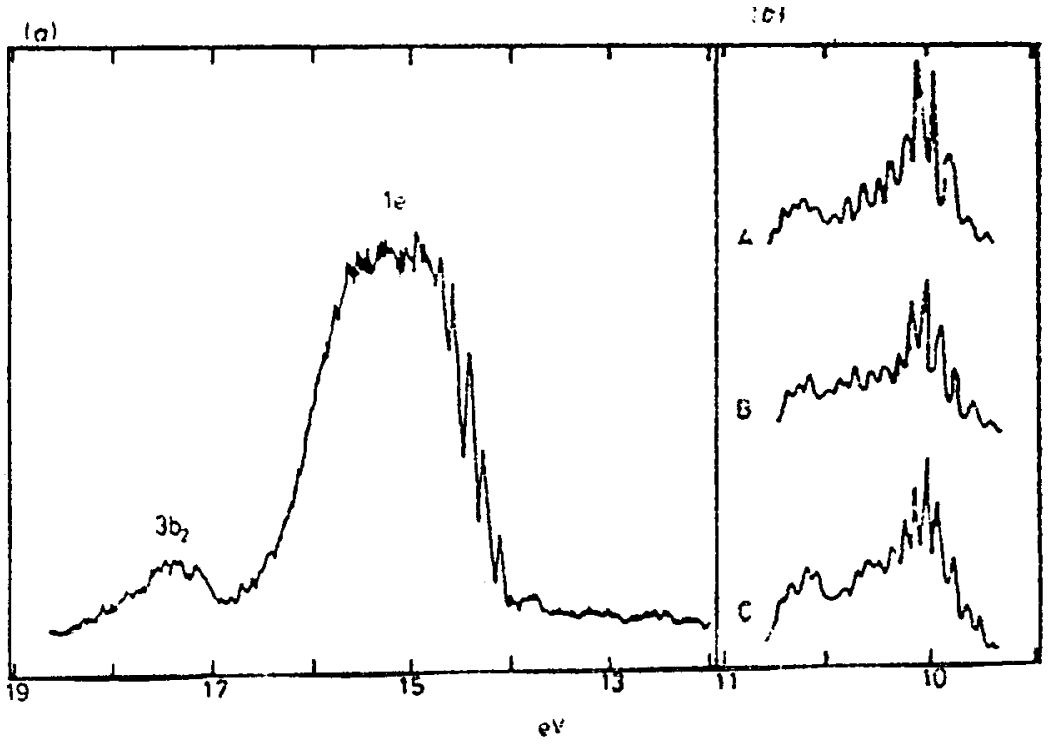

Figure 33.1. The photoelectron spectrum of allene. (*a*) The second and third bands (Turner *et al* 1970). (*b*) The first bands of allene (curve A); allene-1,1-D_2 (curve B), and allene-D_4 (curve C) (Thomas and Thompson 1974). The first bands show evidence of the dynamic Jahn–Teller effect as there are two humps at 10·0 and 10·6 eV.

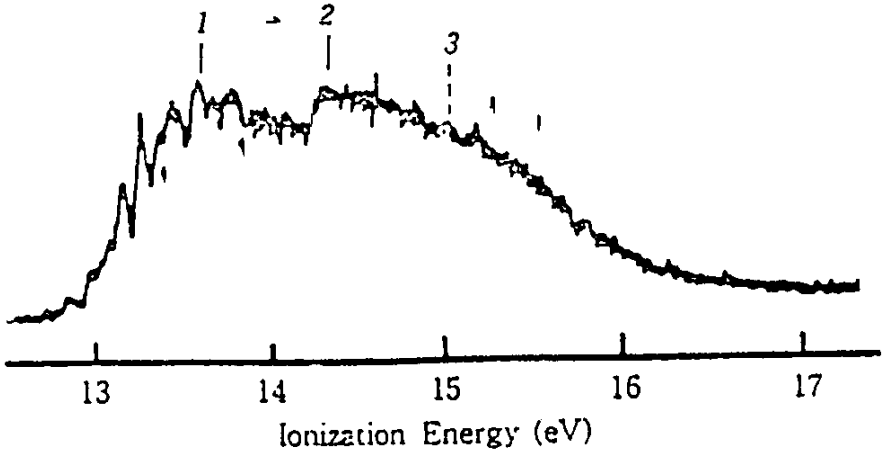

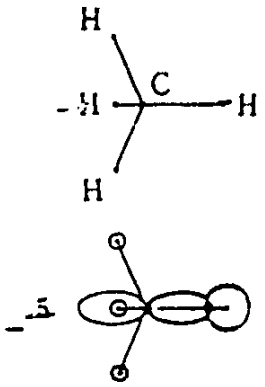

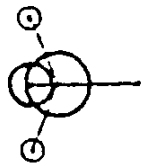

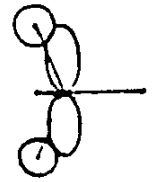

$1sa_1^2 \quad 2sa_1^2\, 2pt_2^6 \qquad\qquad 1A_1$

$CH_4 \xrightarrow{h\nu} CH_4^+ (T_d)$

- $CH_4^+ (^2A_1, C_{3V})$
- $CH_4^+ (^2E, C_{3V})$ → Further to C_{2v}

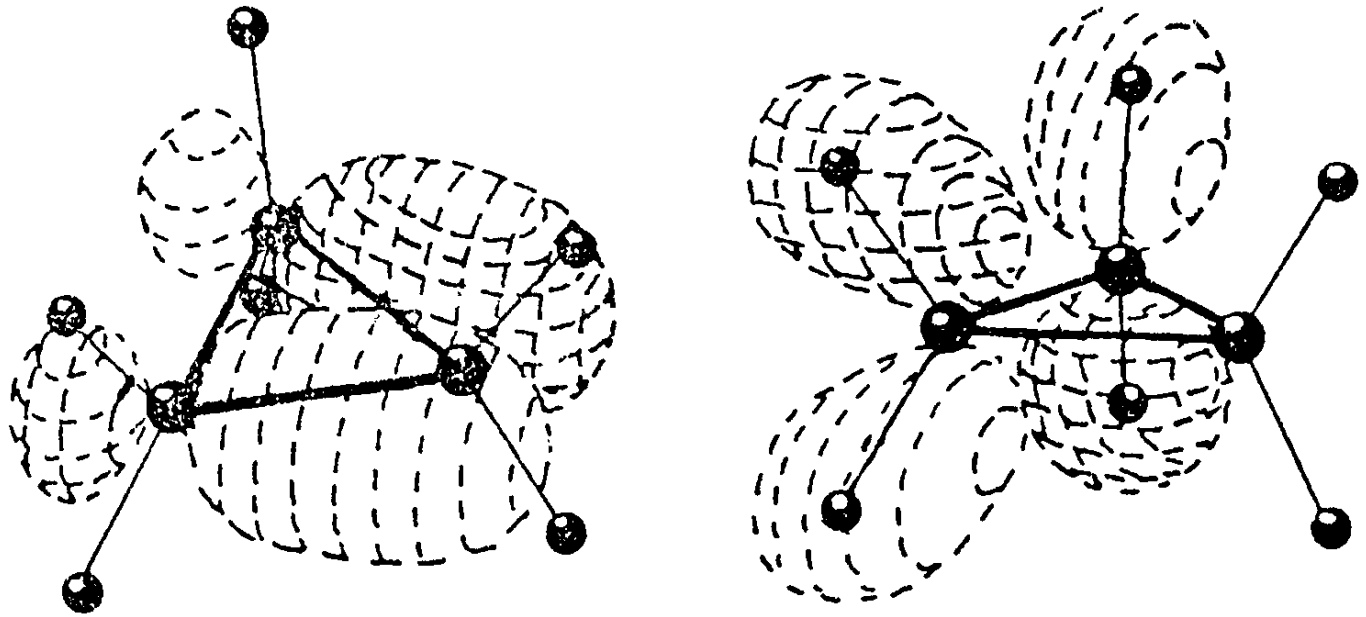

Figure 35.1. The upper occupied orbitals of cyclopropane. Doubly hatched lobes are of the opposite sign to those that are singly hatched.

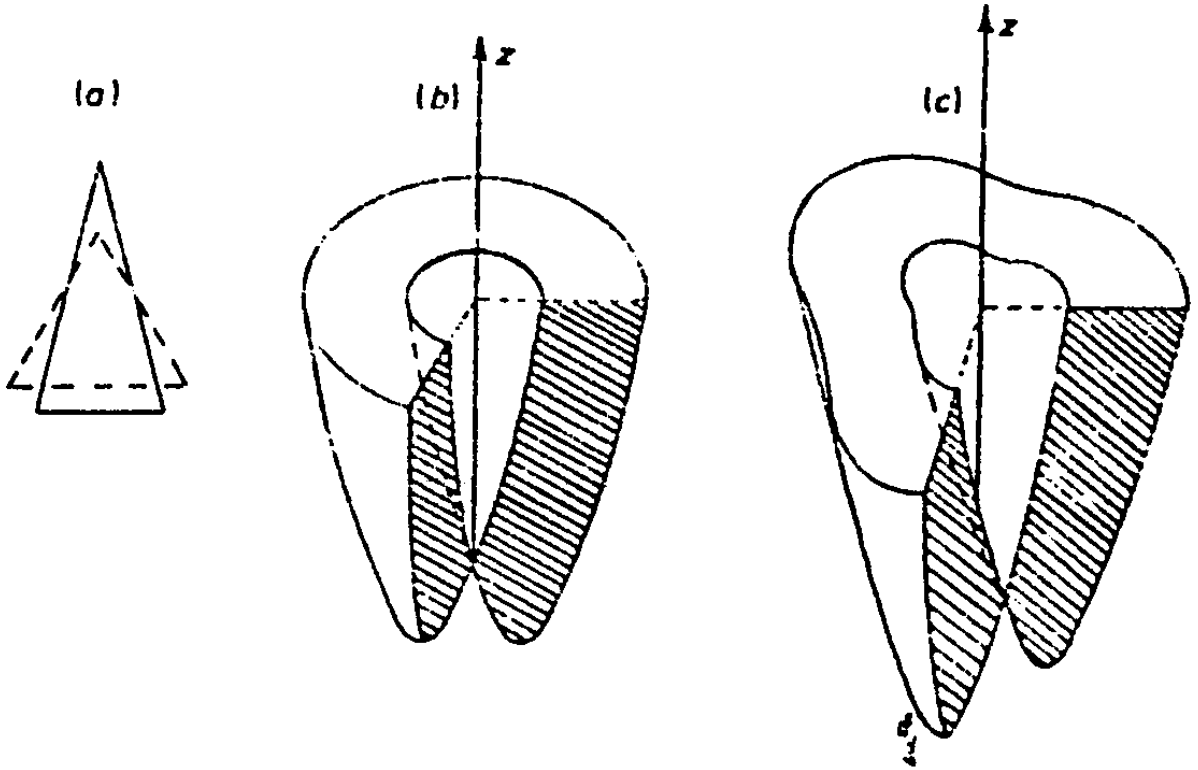

Figure 35.2. (*a*) e′ vibrations produce the maximum Jahn–Teller splitting for the distortion from equilateral to isosceles geometry. (*b*) The axially symmetric energy surfaces obtained with equation (34.3) with the addition of a term for the Hooke's law energy, $\frac{1}{2}kQ^2$. Two surfaces are seen to become degenerate at the z axis. (*c*) Potential energy surfaces of trigonal symmetry obtained from equation (35.4) (Longuet-Higgins 1961).

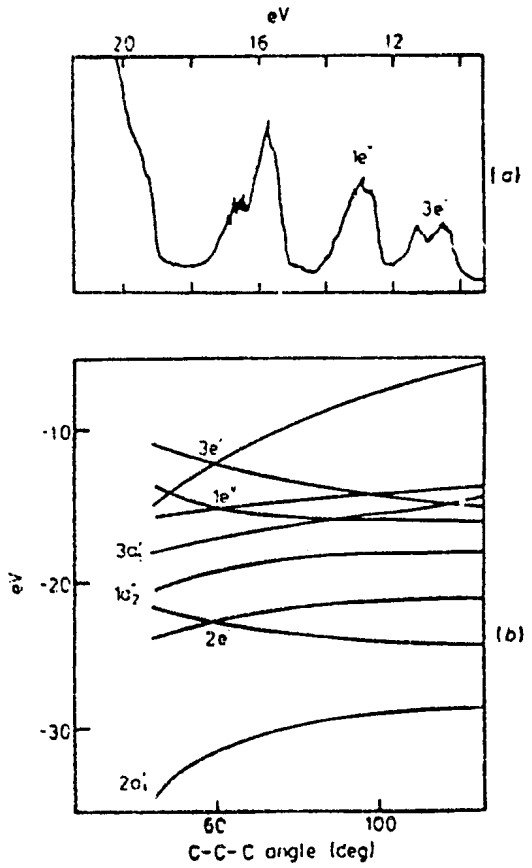

Figure 35.3. (*a*) The photoelectron spectrum of cyclopropane (gas phase) at 20·21 eV (Basch *et al* 1969). (*b*) Walsh diagram for cyclopropane (Buenker and Peyerimhoff 1974). The energy eigenvalues of the orbitals are plotted against the C–C–C angle.

Complex Molecules

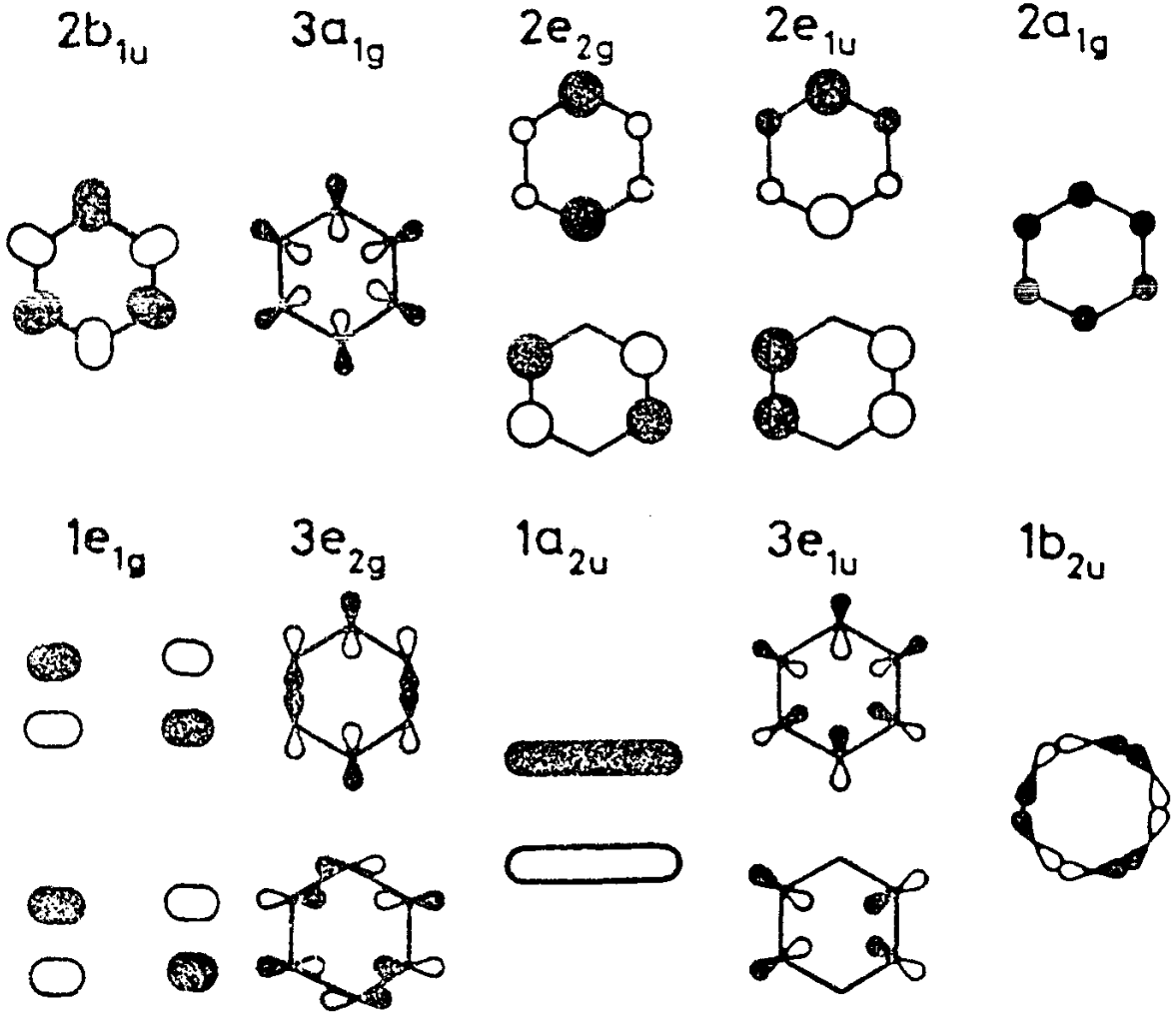

PIPICO

MS – Fragmentation

Theory

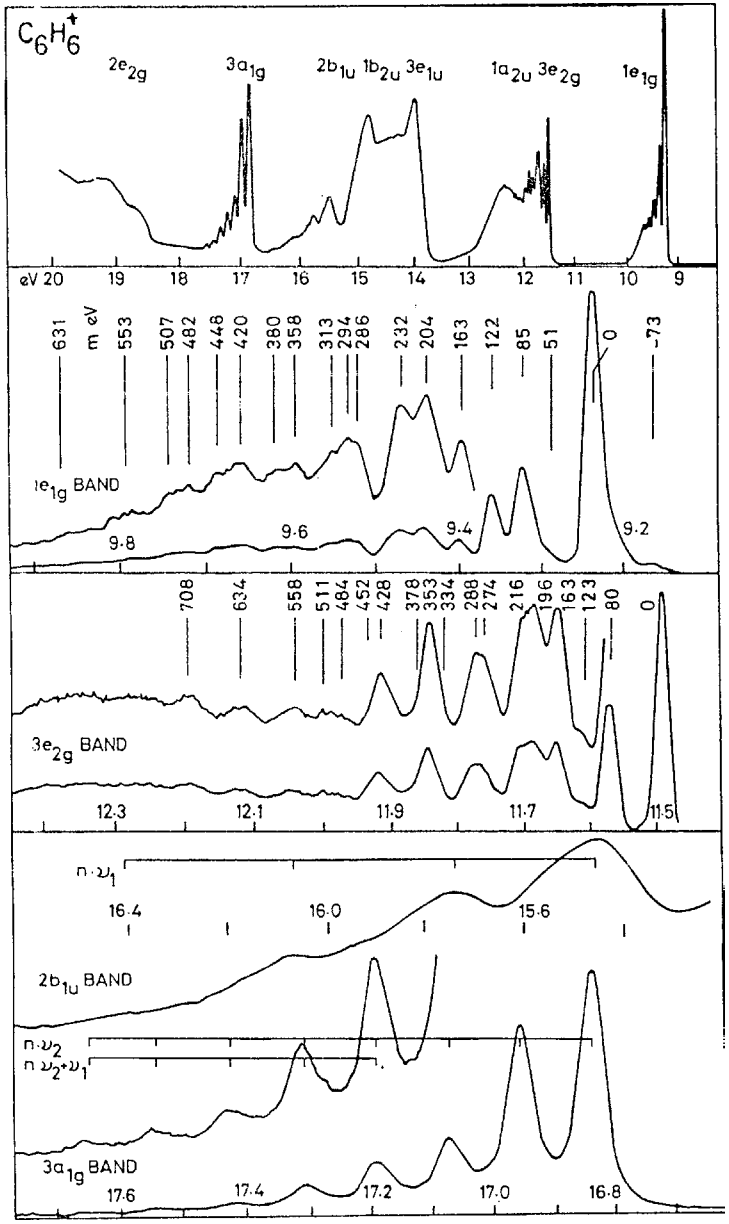
C6H6+
2e2g
3a1g
2b1u 1b2u 3e1u
1a2u 3e2g
1e1g
eV 20 19 18 17 16 15 14 13 12 11 10 9
m eV
631 553 507 482 448 420 380 358 313 294 286 232 204 163 122 85 51 0 -73
1e1g BAND
9·8 9·6 9·4 9·2
708 634 558 511 484 452 428 378 353 334 288 274 216 196 163 123 80 0
3e2g BAND
12·3 12·1 11·9 11·7 11·5
n·ν1
16·4 16·0 15·6
2b1u BAND
n·ν2
n ν2+ν1
3a1g BAND
17·6 17·4 17·2 17·0 16·8

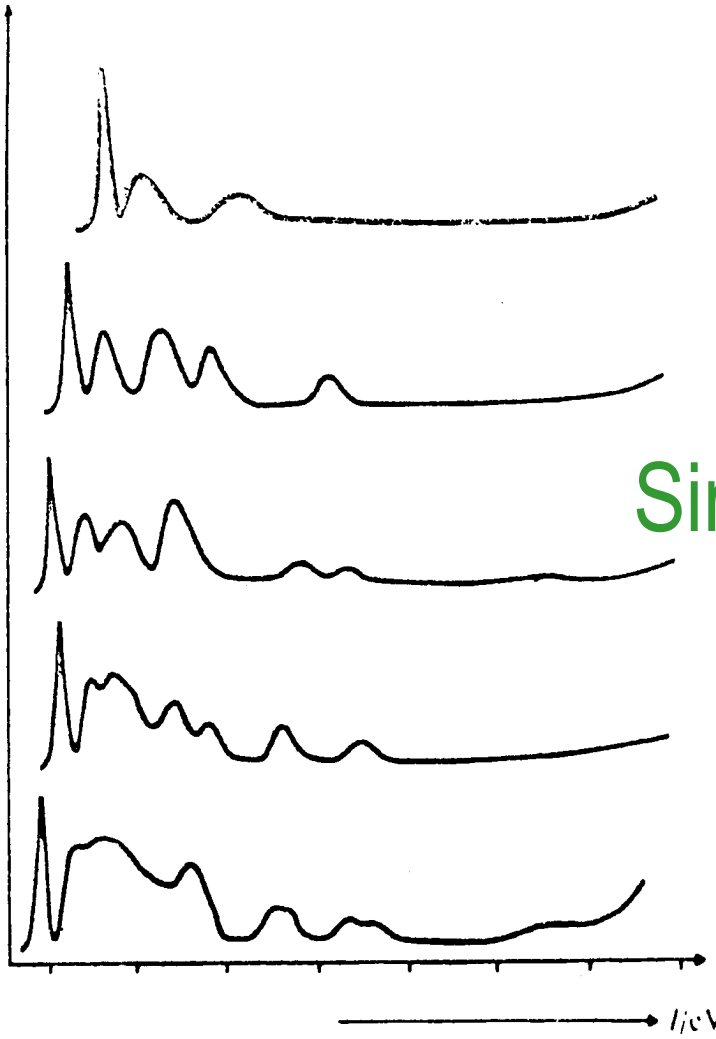

Figure 20.56 He II PE spectra of H_2O and a number of alcohols and ethers.

Simple empirical rules

Complex molecules

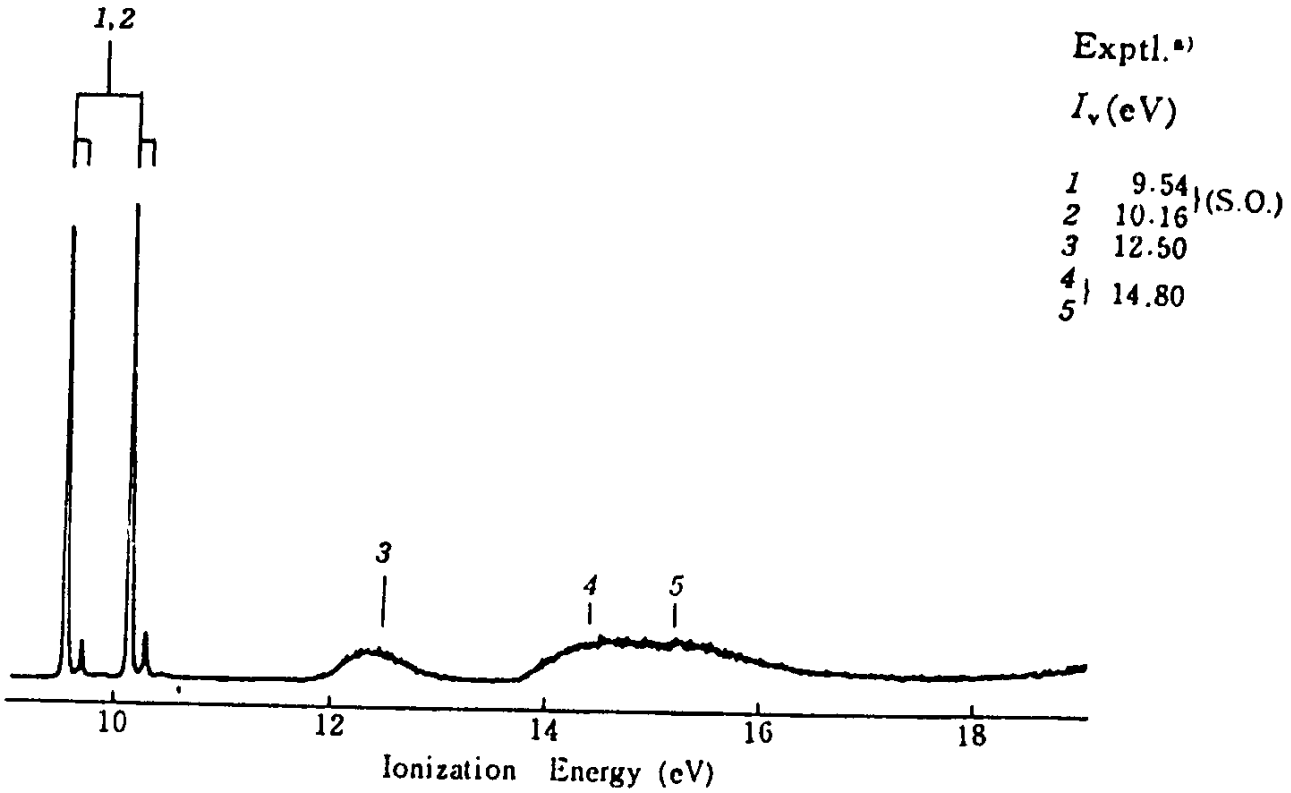

a) Kimura *et al.* (129a). See also other works: Potts *et al.* (176); Ragle *et al.* (192); Turner (213); Uehara *et al.* (216); and Dromey and Peel (86).

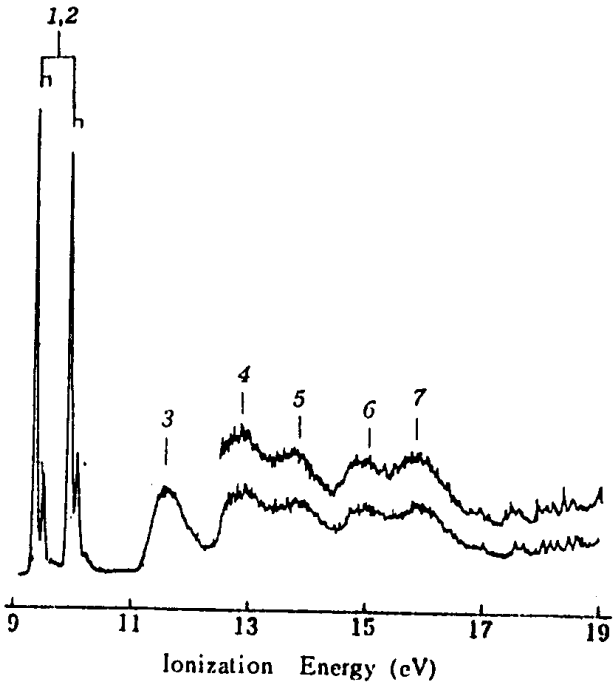

Exptl.[a)]

I_v (eV)

1	9.35	(S.O.)
2	9.93	(S.O.)
3	11.66	
4	12.97	
5	13.84	
6	15.03	
7	15.88	

a) Kimura *et al.* (129a). See also other works: Dromey and Peel (86); Boschi and Salahub (34); Baker *et al.* (9); and Kimura *et al.* (129).

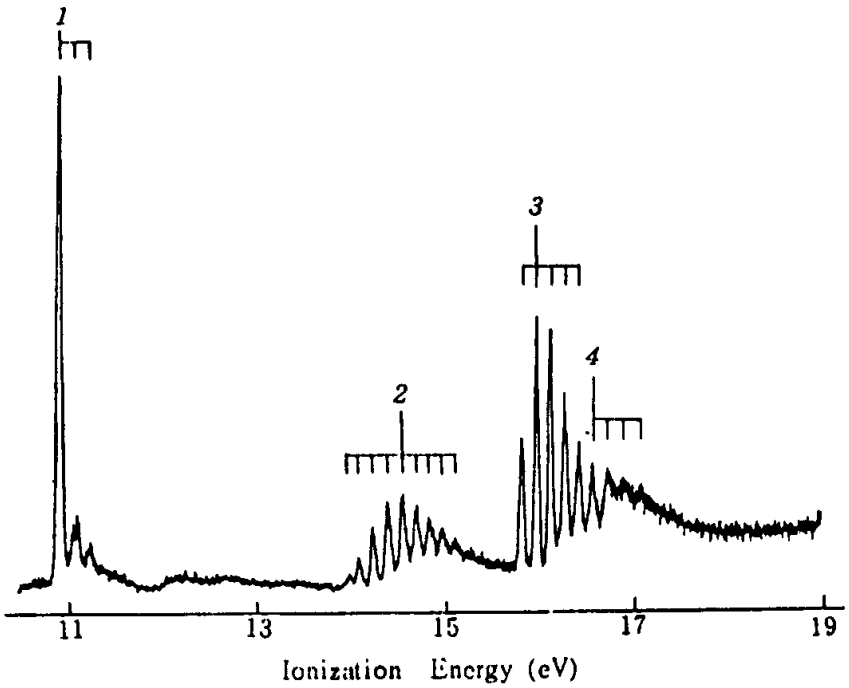

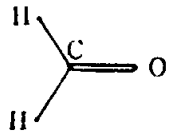

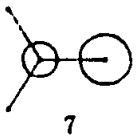

7

9
(vacant)

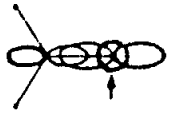

6

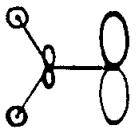

8

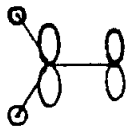

5

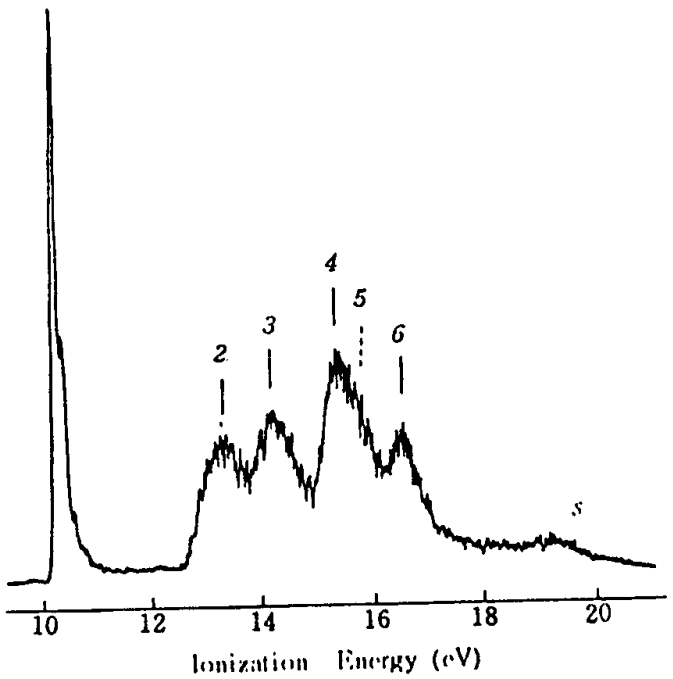

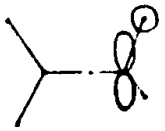

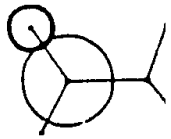

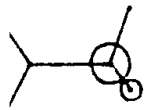

9

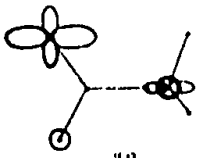

12

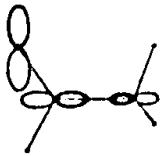

8

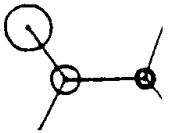

11

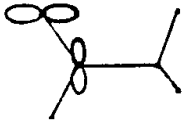

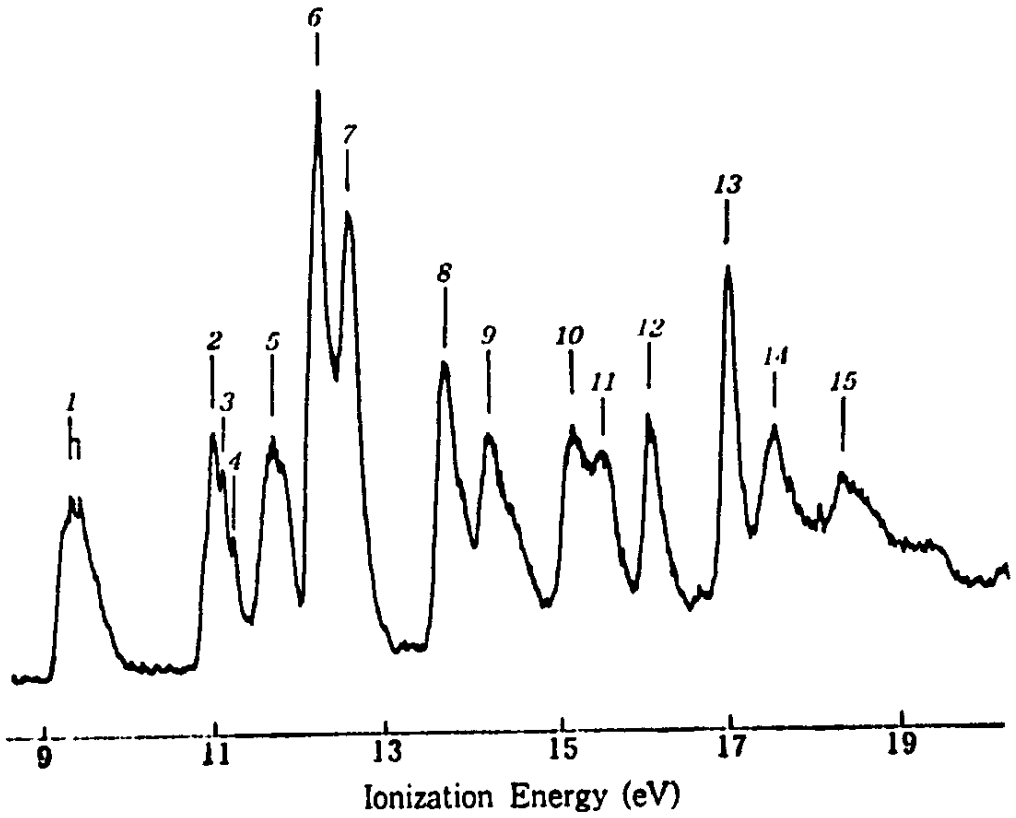

	Exptl.[a] I_v(eV)
1	9.35
2	11.01
3	11.13
4	11.24
5	11.74
6	12.26
7	12.60
8	13.74
9	14.28
10	15.20
11	15.49
12	16.05
13	17.00
14	17.48
15	18.30

a) Kimura *et al.* (129a). See also other work : Streets and Ceasar (206).

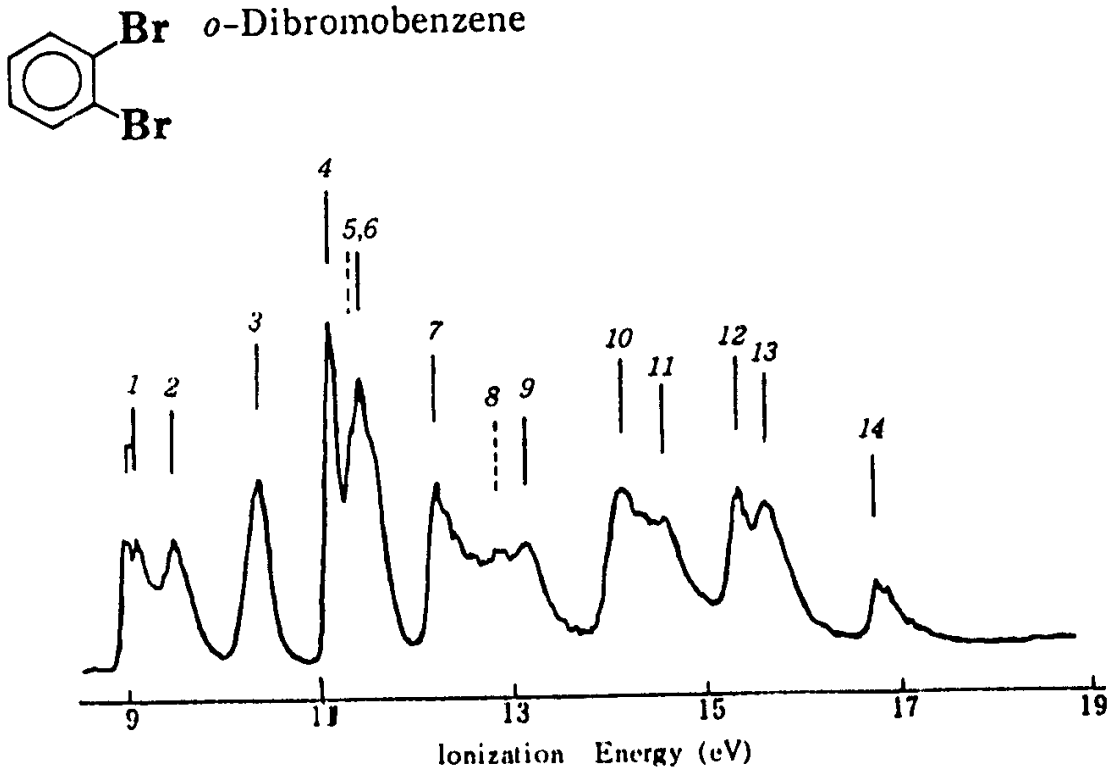

	Exptl.[a] I_v(eV)
1	9.05
2	9.45
3	10.33
4	11.08
5	(11.3)
6	11.38
7	12.15
8	(12.8)
9	13.10
10	14.06
11	14.50
12	15.28
13	15.59
14	16.71

a) Kimura *et al.* (129a). See also other work : Streets and Ceasar (206).

(106) CH_3NH_2 Methylamine

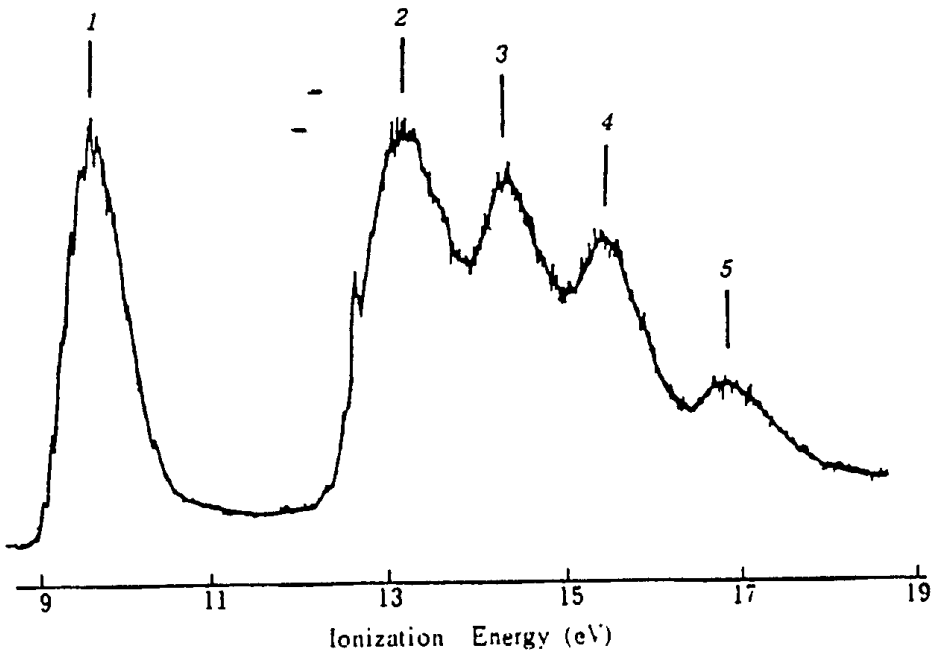

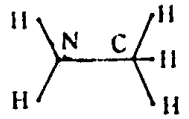

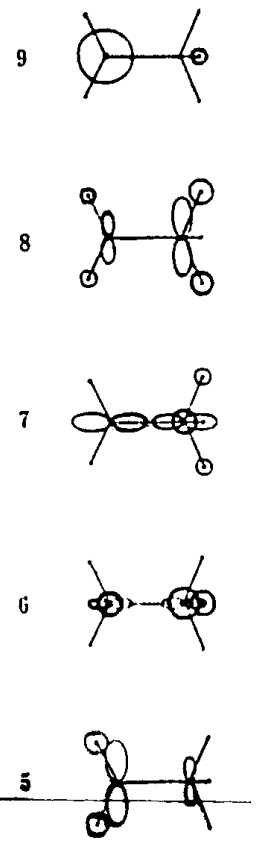

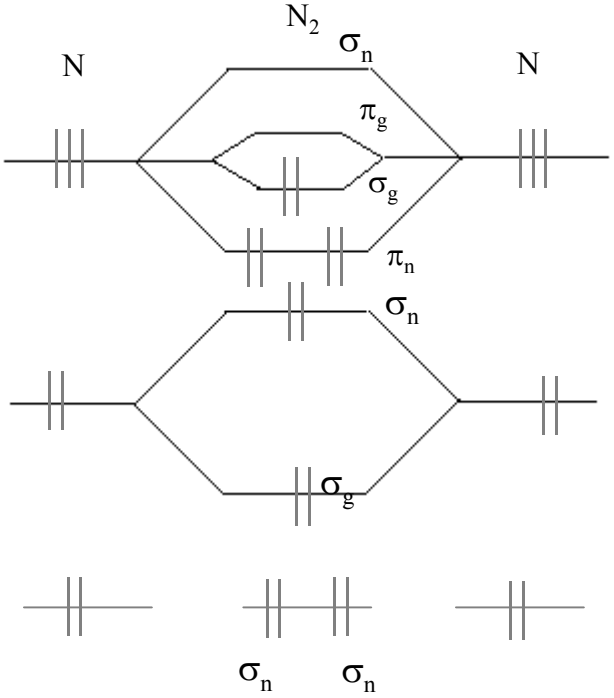
N2
σn
N
N
πg
σg
πn
σn
σg
σn
σn

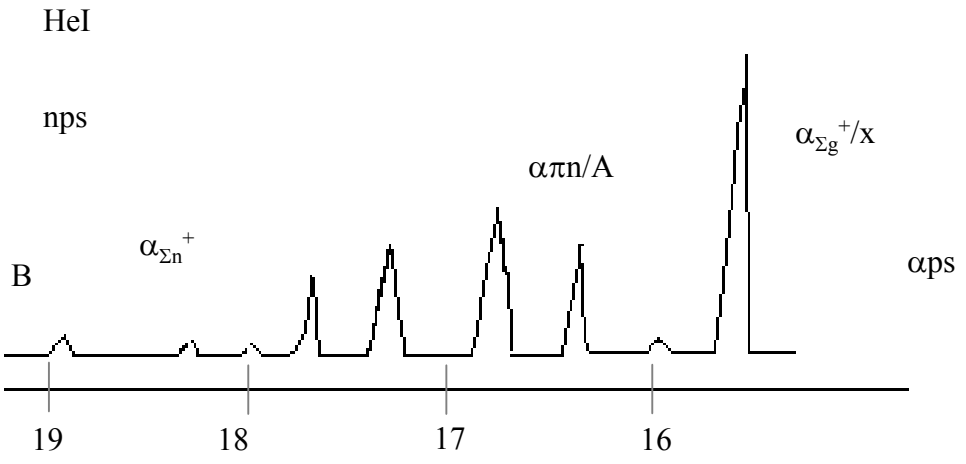
HeI
nps
B
αΣn+
απn/A
αΣg+/x
αps
19
18
17
16

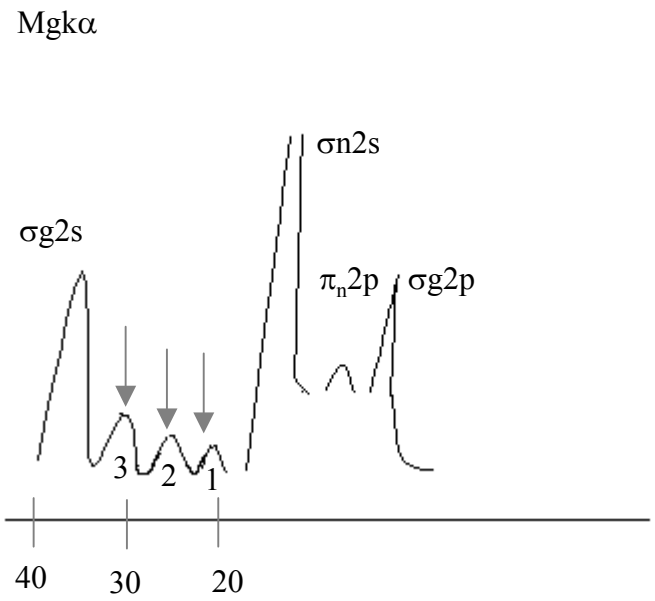
Mgkα
σn2s
σg2s
πn2p
σg2p
3
2
1
40
30
20

From an evaluation of molecular orbitals, it is possible to assign the photoelectron spectrum. Cross sections of orbitals vary substantially and therefore, intensities are different. Cross sections for 2s subshell is an order of magnitude larger than for 2p for Mg K_α. This is known from photoionization studies of Ne. Looking at the Mg K_α spectrum, it is seen that $\sigma_n 2s$ has largest 2s character. The 2s character is in the order $\sigma_u 2s > \sigma_g 2s > \sigma_g 2p$. $\pi_u 2p$ cannot have s character due to symmetry reasons.

$\sigma_g 2s$ is broad $\rightarrow$ vibrational, Coster- Kronig.

Peaks marked by arrows are not due to direct photoemission.

1. shake-up of $\sigma_u 2s$ 2. $MgK\alpha_{3,4}$ 3. Energy loss of $\sigma_u 2s$.000